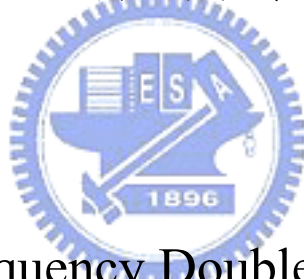


國立交通大學

電信工程學系

碩士論文

W 頻段倍頻器與開關研製



W-band Frequency Doubler and Switch

研究生：謝牧榮

指導教授：張志揚 博士

中華民國 九十三年 六月

# W-band Frequency Doubler and Switch

研究生：謝牧榮

Student : Mu-Rung Hsieh

指導教授：張志揚 博士

Advisor : Dr. Chi-Yang Chang

國立交通大學

電信工程學系



A Thesis

Submitted to Department of Communication Engineering  
College of Electrical Engineering and Computer Science

National Chiao Tung University

In Partial Fulfillment of the Requirements

for the Degree of  
Master of Science

In

Communication Engineering

June 2004

Hsinchu, Taiwan, Republic of China

中華民國 九十三年 六月

# W 頻段倍頻器與開關研製

研究生：謝牧榮

指導教授：張志揚 博士

國立交通大學電信工程學系



本論文提出適合 77GHz 汽車防撞雷達的倍頻器和開關。在倍頻器的研製中，我們使用電壓電流的關係來分析倍頻器。此外，本文使用並探討一些倍頻器的架構。這些架構包含岔入環、共平面波導 (CPW)-共平面帶線(CPS)之平衡與非平衡轉換器(Balun)以及共平面波導平衡與非平衡轉換器。

本論文也描述了開關設計的原理以及一些開關的架構。其中包括了串聯式、並聯式以及串聯-並聯式的開關。並有實作與量測並聯式的單刀單擲和單刀雙擲開關。倍頻器與開關都使用砷化鎵蕭基二極體以共平面波導的形式製作在三氧化二鋁的基板。

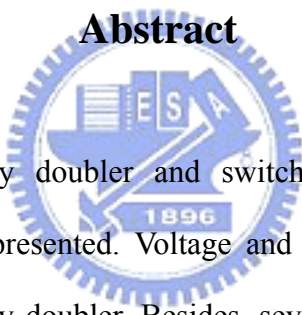
# W-band Frequency Doubler and Switch

Student: Mu-Rung Hsieh

Advisor: Dr. Chi-Yang Chang

Department of Communication Engineering  
National Chiao Tung University

## Abstract

The logo of National Chiao Tung University is a circular emblem with a gear-like border. Inside the circle, there are stylized letters 'E', 'S', and 'A' arranged vertically, and the year '1896' at the bottom. The logo is semi-transparent and overlaid on the abstract text.

In this thesis, frequency doubler and switch for 77GHz vehicle-collision-avoidance-radar-system are presented. Voltage and current relationship is used to qualitatively analyze frequency doubler. Besides, several circuit structures including rat-race ring coupler, coplanar waveguide (CPW)-coplanar strip (CPS) balun, and CPW balun, are adopted and discussed.

The theory of switch design is also described. Some configurations of switch are introduced such as series, shunt, and series-shunt configuration. The Shunt configured switch of SPST and SPDT are implemented and measured. Both frequency doubler and switch are fabricated with commercial GaAs Schottky diode on  $\text{Al}_2\text{O}_3$  substrate in CPW.

# Acknowledgment

## 誌謝

首先要感謝指導教授張志揚博士在兩年的時間中辛勤地指導與鼓勵，老師在微波電路豐富的知識與經驗使學生在學業上獲益良多。同時要感謝口試委員邱煥凱教授、楊正任教授及鍾世忠教授的不吝指導得以使得此篇論文更為完善。另外要謝謝中科院三所七組協助完成薄膜電路的製作及量測。

感謝實驗室的學長姊及同窗好友俊毅、鈞翔、湘竹、澤民和實驗室的學弟妹們，因為有你們的陪伴，讓我能在融洽的實驗室裡，度過我充實的研究生生涯。另外還有我的大學同學揚裕、禮鈞以及多年共處的室友傑閔、宏霖、稚峰、盈良、柏成，因為你們讓我的生活添加了許多色彩。當然最後要感謝陪我一路走來的家人，媽、乾媽、弟弟，你們的支持是我做研究最大的動力，謝謝你們一直在我身邊陪伴我、鼓勵我，我要把我的研究成果獻給他們。

# Contents

<b>Abstract (Chinese)</b> .....	<b>I</b>
<b>Abstract</b> .....	<b>II</b>
<b>Acknowledgment</b> .....	<b>III</b>
<b>Contents</b> .....	<b>IV</b>
<b>List of figure</b> .....	<b>V</b>
<b>Chapter 1 Introduction</b> .....	<b>1</b>
<b>Chapter 2 Frequency doubler</b> .....	<b>3</b>
<b>2.1 Rat-race ring frequency doubler</b>	
<b>2.1.1 Circuit analysis</b> .....	<b>3</b>
<b>2.1.2 Circuit implementation and measurement</b> .....	<b>8</b>
<b>2.2 CPW to CPS transition Balun-type frequency doubler</b>	
<b>2.2.1 Circuit analysis</b> .....	<b>14</b>
<b>2.2.2 Circuit implementation and measurement</b> .....	<b>19</b>
<b>2.3 Broadband CPW balun-type doubler</b>	
<b>2.3.1 Circuit analysis</b> .....	<b>24</b>
<b>2.3.2 Circuit implementation and measurement</b> .....	<b>27</b>
<b>Chapter 3 Switch</b> .....	<b>31</b>
<b>3.1 Theory of Switch design</b> .....	<b>31</b>
<b>3.2 Circuit implementation and measurement</b> .....	<b>44</b>
<b>Chapter 4 Conclusion</b> .....	<b>49</b>
<b>References</b> .....	<b>50</b>

# List of Figure

Fig2.1-1 Circuit and s-parameter of traditional rat-race ring coupler.....	3
Fig2.1-2 Rat-race ring frequency doubler configured with diodes in reverse direction.....	4
Fig2.1-3 Graphical analysis of voltage and current of diodes in reverse direction.....	5
Fig2.1-4 Rat-race ring frequency doubler configured with diodes in same direction.....	6
Fig2.1-5 Graphical analysis of voltage and current relationship of diodes in same direction...	7
Fig2.1-6 Physical layout of the rat-race ring frequency doubler.....	9
Fig2.1-7 Measured conversion loss versus frequency of the rat-race ring doubler	
(a) Diodes in the reverse direction.....	9
(b) Diodes in the same direction.....	10
Fig2.1-8 Measurement of conversion loss versus input power at 77GHz of the rat-race ring doubler	
(a) Diodes in the reverse direction.....	10
(b) Diodes in the same direction.....	11
Fig2.1-9 Measured conversion loss of the rat-race ring doubler with diodes in the reverse direction in the whole band.....	13
Fig2.1-10 Measured isolation of the rat-race ring doubler with diodes in the reverse direction in the whole band.....	13
Fig2.2-1 Physical layout of CPW to CPS transition balun.....	14
Fig2.2-2 The measurement of back-to-back connected CPW-CPS balun.....	15
Fig2.2-3 Circuit model of balun.....	15
Fig2.2-4 Circuit model of balun-type doubler with diodes in the reverse direction.....	16
Fig2.2-5 Voltage and current relationship of balun-type doubler.....	17
Fig2.2-6 Circuit model of balun-type doubler with diodes in the same direction.....	18
Fig2.2-7 Voltage and current relationship of balun-type doubler with diodes in the same	

direction.....	18
Fig2.2-8 Balun-type doubler layout with diodes configured in the reverse direction.....	19
Fig2.2-9 Measured conversion loss of balun-type doubler with diodes in reverse direction...	20
Fig2.2-10 Balun-type doubler layout with diodes configured in the same direction.....	21
Fig2.2-11 The measured conversion loss of balun-type doubler with diodes in the same direction.....	21
Fig2.2-12 Measurement of conversion loss versus input power at 77GHz of the CPW-CPS balun doubler.....	23
Fig2.2-13 Broadband measurement of conversion loss of CPW-CPS balun type doubler with diodes in the same direction.....	23
Fig2.3-1 The schematic of the CPW balun-type doubler.....	24
Fig2.3-2 E-field distribution of CPW balun.....	24
Fig2.3-3 Simulated result of CPW balun	
(a) Simulated magnitude response of CPW balun.....	25
(b) Simulated phase response of CPW balun.....	25
Fig2.3-5 The circuit model of CPW balun-type doubler.....	26
Fig2.3-6 The voltage and current relationship of CPW balun-type doubler.....	26
Fig2.3-7 Physical layout of CPW balun-type doubler.....	27
Fig2.3-8 Measurement of CPW balun-type doubler	
(a) Broad band measurement of conversion loss response.....	28
(b) Broad band measurement of isolation response.....	28
Fig2.3-9 Simulation of doubler resonance	
(a) Circuit model of doubler resonance (b) Simulated response of resonance.....	29
Fig2.3-10 Non-linear simulation of CPW balun doubler including bond wire parasitic effect and twisted line	
(a) Circuit model of doubler including parasitic effect.....	30



(b) Simulated conversion of CPW balun-type doubler including parasitic effect.....	30
Fig3-1 Switch configuration.....	32
Fig3-2 Two classifications of switches.....	33
Fig3.3 Reflective switch configurations for SPDT.....	33
Fig3-4 Measured impedance of Schottky diode under forward and reverse biasing.....	37
Fig3-5 Complex conjugate pairs in the Smith chart.....	39
Fig3-6 Transformed impedances with 180° difference.....	39
Fig3-7 Final impedance of forward and reverse biasing.....	40
Fig3-8 Simulated matching network in HFSS.....	41
Fig3-9 Curve fitting between ideal and practical matching network.....	41
Fig3-10 Shunt configured SPST simulation	
(a) SPST simulation (b) Simulated insertion loss and isolation of SPST.....	42
Fig3-11 Shunt configured SPDT simulation	
(a) SPDT simulation (b) Simulated insertion loss and isolation of SPDT.....	43
Fig3-12 Physical layout of shunt configured SPST and SPDT	
(a) Shunt configured SPST (b) Shunt configured SPDT.....	44
Fig3-13 Measurement of shunt configured SPST	
(a) Measured isolation and insertion loss of shunt configured SPST.....	45
(b) Measured return loss at ON and OFF state of shunt configured SPST.....	45
Fig3-14 Measurement of shunt configured SPDT	
(a) Measured isolation and insertion loss of shunt configured SPDT.....	46
(b) Measured return loss at ON and OFF state of shunt configured SPDT.....	46
Fig3-15 The effect of the bond wire location	
(a) Location Variation of bond wire.....	48
(b) Various simulation result correspond to different bond wire location.....	48

# Chapter 1 Introduction

More and more commercial applications have been designated at millimeter wave frequency range in recent years. 28GHz local-multipoints-delivery-system (LMDS), 60GHz wireless local-area-network (WLAN), and 77GHz vehicle-collision-avoidance-radar system are typical and well-known applications. For example, the 77GHz vehicle-collision-avoidance-radar system could provide safety applications such as collision warning, airbag pre-crash sensing, and parking aid. The increasing trend of application realized at millimeter wave highlights the importance of components at W-band. This thesis focuses on two components in vehicle-collision-avoidance-radar system, namely, the 77GHz frequency doubler and the 77GHz switches.

The uniplanar circuit topology is suitable for MIC and MMIC due to its low cost and easy integration. Therefore, the frequency doubler and switch are implemented in coplanar waveguide (CPW). Besides, coplanar waveguide has following advantages [1].

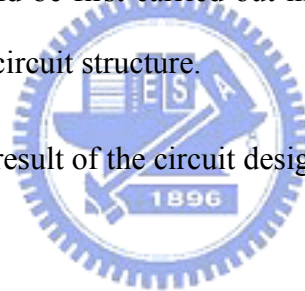
First, CPW can realize the series network as easy as shunt network with surface mounting devices. Second, it eliminates the need for via holes. Third, the characteristic impedance is determined by the ratio of the line width and the gap between signal and ground. This makes circuit design more flexible. Moreover, it reduces radiation loss and cross talk effects.

Both frequency doubler and switch are realized with beam lead GaAs Schottky diodes and fabricated on a  $\text{Al}_2\text{O}_3$  substrate with dielectric constant of 9.8 and substrate thickness of 15mils. Chapter 2 and 3 would describe these two components respectively.

In chapter 2, three types of frequency doublers are proposed. They can be further categorized into two kinds of structures: magic-T type and balun (balanced-to-unbalanced transformer) type. In a generalized point of view, both types want to reach the functionality that feeds the fundamental signal to Schottky diode and produces the 2<sup>nd</sup> harmonic signal due to the non-linearity of the diodes. The thesis will adopt the voltage and current relationship of Schottky diode to qualitatively analyze the frequency doubler.

In chapter 3, the switches are presented. Vehicle-collision-avoidance-radar-system has to detect three directions of signal in the front side of the vehicle. There are three antennas in the RF front end. Therefore, a single-pole-triple-throw (SP3T) is needed. SPST and SP2T would be first carried out in order to see whether the SP3T could be implemented in this circuit structure.

Chapter 4 concludes the result of the circuit design of these two components.



## Chapter 2 Frequency doubler

This chapter is divided into two parts: part I for magic T-type frequency doubler and part II for balun-type one. I will first introduce the circuit structure in each part, and then analyze the measurement to see how it works.

### Part I : Magic T-type

#### 2.1 Rat-race ring frequency doubler

##### 2.1.1 Circuit analysis

Rat-race ring is a coupler containing a sum port and a delta port. When a signal enters the sum port, the coupler will split the signal to two output ports with equal magnitude and equal phase. On the other hand, when a signal enters the delta port, the coupler splits it to output ports with equal magnitude and out of phase. We can grasp this port property by examining the scattering parameter at center frequency of the traditional rat-race ring in [2]. Fig2.1-1 depicts the traditional rat-race ring coupler.

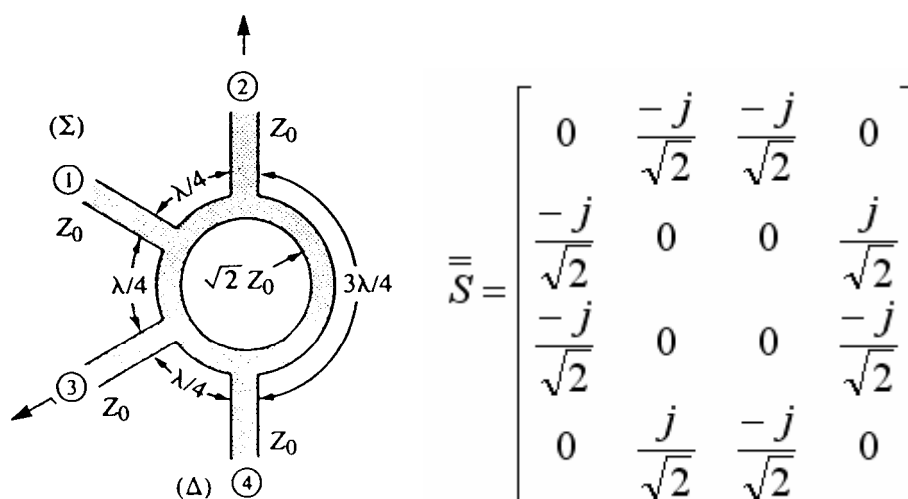


Fig2.1-1 Circuit and s-parameter of traditional rat-race ring coupler

The rat-race ring coupler can be used for frequency doubler by the following configuration shown in Fig2.1-2. The fundamental signal is applied to the sum port of the rat-race ring coupler, and the 2<sup>nd</sup> harmonic signal is obtained at the delta port of the coupler. In this configuration, the Schottky diodes placed at two output ports must be in reverse direction; otherwise the 2<sup>nd</sup> harmonic signal will be cancelled at the output.

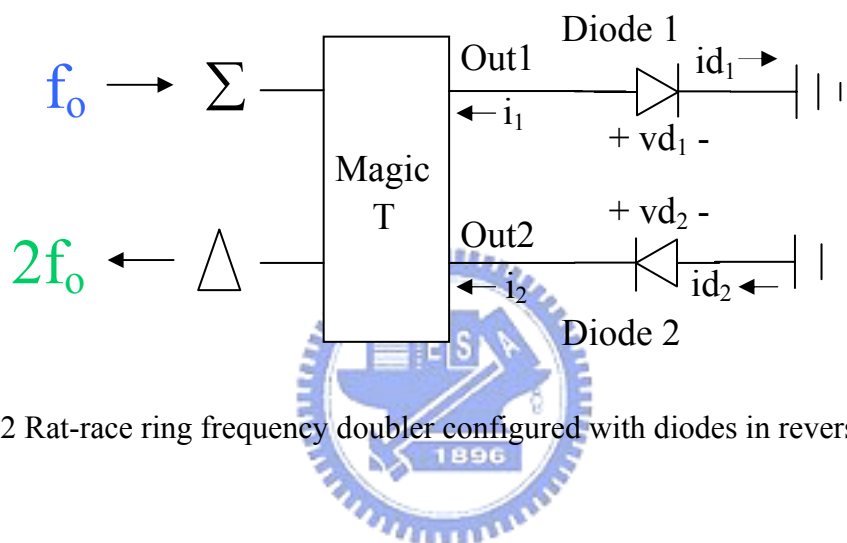


Fig2.1-2 Rat-race ring frequency doubler configured with diodes in reverse direction

Fig2.1-3 qualitatively analyzes the voltage and current relationship in this configuration, so as to see how the rat-race ring coupler cooperates with Schottky diodes to function as a frequency doubler. In the configuration shown in Fig2.1-2, the fundamental signal,  $f_0$ , is delivered to the sum port of the rat-race ring coupler. As mentioned previously, the signal would be divided to two in-phase and equal magnitude imposing upon two diodes.  $v_{d1}$  and  $v_{d2}$ , the voltages across the Schottky diodes therefore have the same waveform in time domain.  $i_{d1}$  and  $i_{d2}$ , the currents in the direction of the forward bias of the diodes, will be turned on in different half period of the input signal due to the different directions of diodes.

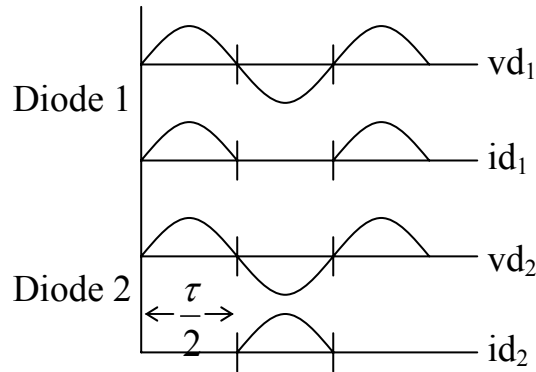


Fig2.1-3 Graphical analysis of voltage and current of diodes in reverse direction

Expand  $id_1$  and  $id_2$  into Fourier series form (2.1) where  $g_n$  is the  $n$ th harmonic term.

$$\left. \begin{aligned}
 id_1 &= \sum g_n e^{jn\omega t} \\
 id_2 &= \sum g_n e^{jn\omega \left(t + \frac{\tau}{2}\right)} = \sum g_n e^{jn\omega t} e^{jn\pi} \\
 id_2^{(n)} &= id_1^{(n)} \cdot (-1)^n
 \end{aligned} \right\} (2.1)$$

Merely considering about the current of the  $2_{nd}$  harmonic term,  $2f_0$ , equation (2.1) shows that  $id_1^{(2)}$  equals  $id_2^{(2)}$ . Since  $i_1 = -id_1^{(2)}$  and  $i_2 = id_2^{(2)}$ , the desired frequency term at the delta port would be  $i_{\Delta} = i_1 - i_2 = -2id_1^{(2)}$  from reciprocity. The desired term at the sum port could be  $i_{\Sigma} = i_1 + i_2 = 0$ . Hence, we can foresee that  $2f_0$  would only go through the delta port. As for the fundamental term, the isolation of magic T between sum port and delta port is ideally infinite by nature. Consequently,  $f_0$  won't go through the sum port.

If the diodes in Fig2.1-2 are in the same direction, the currents of the diodes are derived as  $id_2^{(n)} = id_1^{(n)} * (1)^n = id_1^{(n)}$ . The output current of  $2f_0$  at the delta port would be  $i_{\Delta} = i_1 - i_2 = 0$ . The desired term thus disappears and the rat-race ring is no more a doubler.

Actually, we can also obtain  $2f_0$  from the sum port if we feed  $f_0$  to the delta port and modify the direction of the diodes as Fig2.1-4.

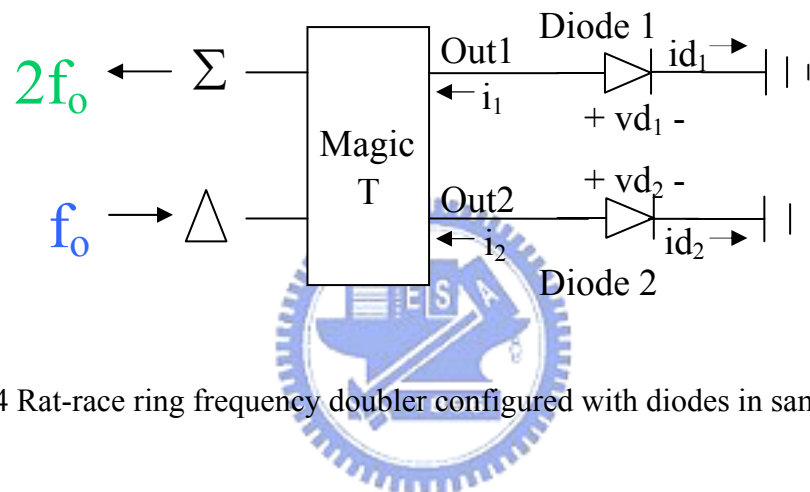


Fig2.1-4 Rat-race ring frequency doubler configured with diodes in same direction

The same analysis of the voltage and current relationship of the diodes is illustrated in Fig2.1-5 when the circuit is configured as Fig2.1-4. As the fundamental signal is delivered to the delta port, the magic T would split it into two signals with equal magnitude and out-of-phase. Thus,  $vd_1$  and  $vd_2$  will differ from each other with a half period in the time domain, and  $id_1$  and  $id_2$  will be turned on as the diode is forward biased respectively.

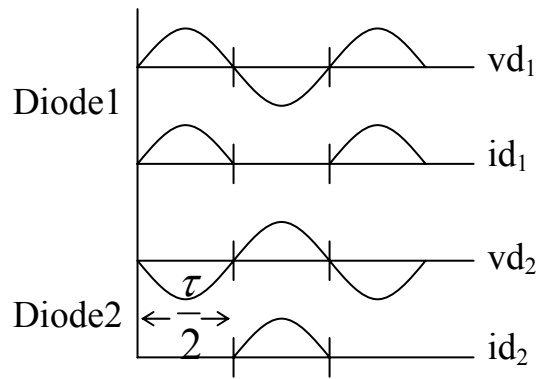


Fig2.1-5 Graphical analysis of voltage and current relationship of diodes in same direction

Expand  $id_1$  and  $id_2$  into Fourier series form (2.2).

$$\begin{aligned}
 id_1 &= \sum g_n e^{jn\omega t} \\
 id_2 &= \sum g_n e^{jn\omega \left(t + \frac{\tau}{2}\right)} = \sum g_n e^{jn\omega t} e^{jn\pi} \\
 id_2^{(n)} &= id_1^{(n)} \cdot (-1)^n
 \end{aligned}
 \tag{2.2}$$

Considering only the  $2^{nd}$  harmonic term,  $id_1^{(2)}$  equals  $id_2^{(2)}$ . Since  $i_1 = -id_1^{(2)}$  and  $i_2 = -id_2^{(2)}$ , the desired frequency term at the sum port would be  $i_\Sigma = i_1 + i_2 = -2id_1^{(2)}$  from reciprocity. The desired term at the delta port could be  $i_\Delta = i_1 - i_2 = 0$ . Hence, we can predict the  $2f_0$  term would only go through the sum port. Again, the  $f_0$  won't go through the sum port, since the isolation between sum port and delta port is ideally infinite by nature.

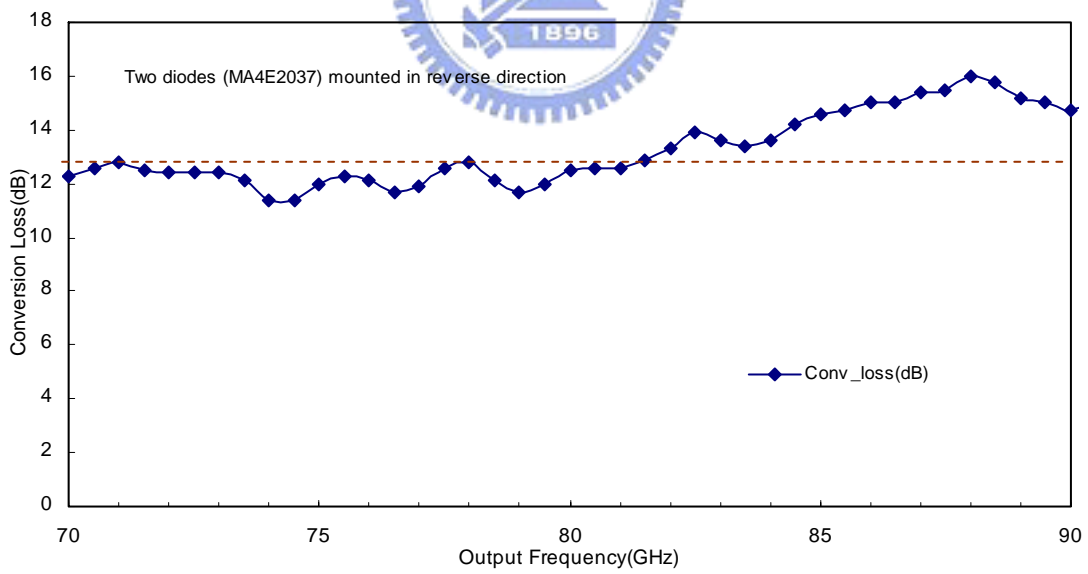
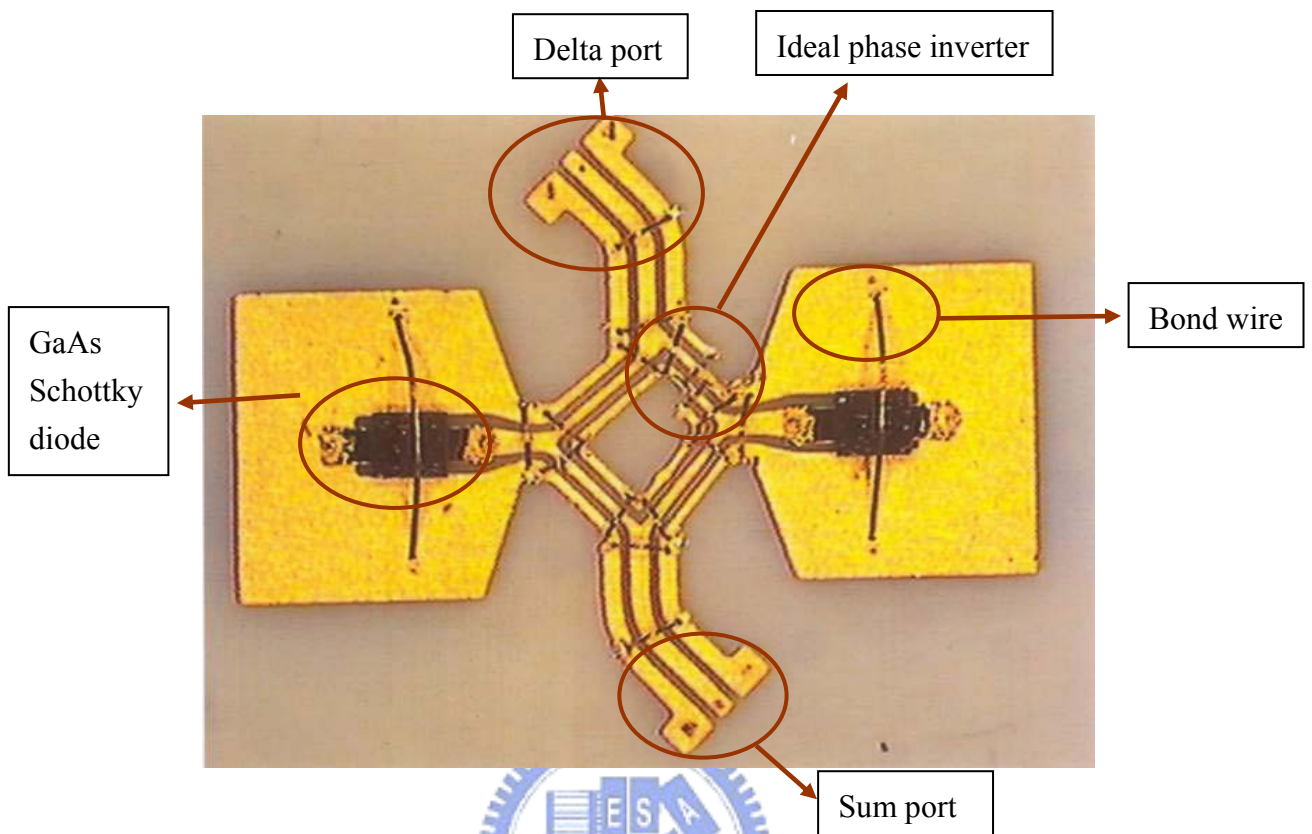
A well-configured magic T is not ready to realize a frequency doubler. The bandwidth of the magic T should cover an octave frequency band. If the bandwidth is not wide enough, the performance of the rat-race ring frequency doubler will degrade seriously. Therefore, a rat-race ring coupler, which covers at least an octave frequency



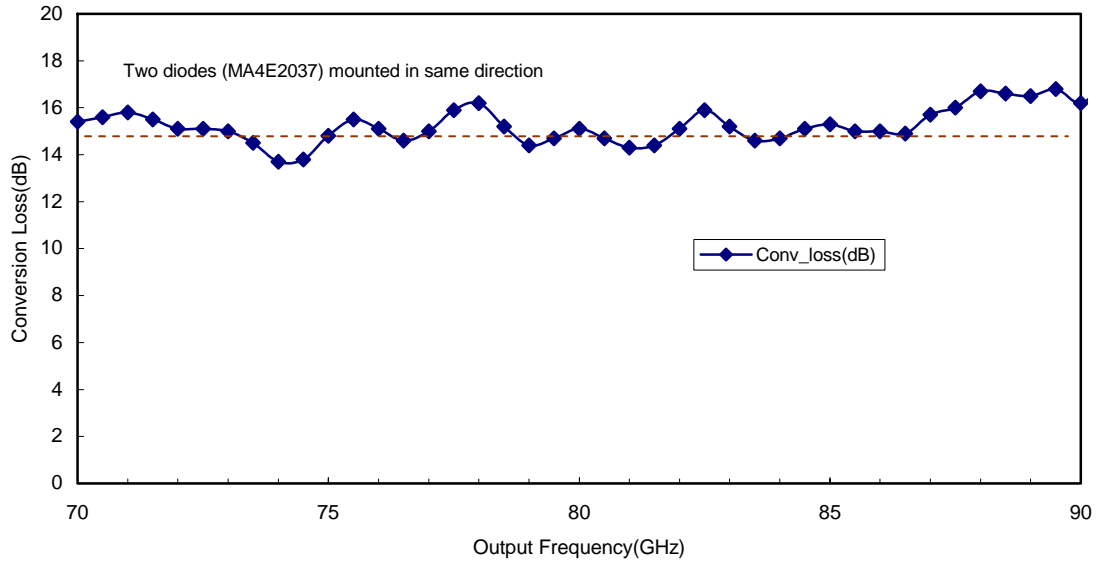
band, is needed. The traditional rat-race ring coupler could cover only bandwidth on the order of 20%~30%. Many efforts have been done to make the bandwidth of the rat-race ring coupler wider in [3]~[6]. In [3], the three-quarter-wavelength line is replaced by a short-circuited quarter-wave coupled-line. The short-circuited coupled-line performs as a section of transmission line preceded by an ideal phase-inverting transformer. In [4], the phase inversion is achieved by utilizing the field nature at the CPW-slotline T-junction. In [5] and [6], a twisted line is adopted to realize the ideal phase inversion. The rat-race ring couplers mentioned above all perform well in a broad bandwidth.

### **2.1.2 Circuit implementation and measurement**

A rat-race ring with twisted line, an ideal phase inverter, could achieve the bandwidth requirement of frequency doubler. This equips rat-race ring coupler for a frequency doubler. The rat-race ring frequency doubler based on [6] would be implemented and measured. Fig2.1-6 is the physical layout of the rat-race ring frequency doubler. The circuit size is about 95mil x 116mil. Fig2.1-7(a) and (b) are the measured conversion loss versus frequency of the rat-race ring frequency doubler with Schottky diodes in reverse and same direction respectively.



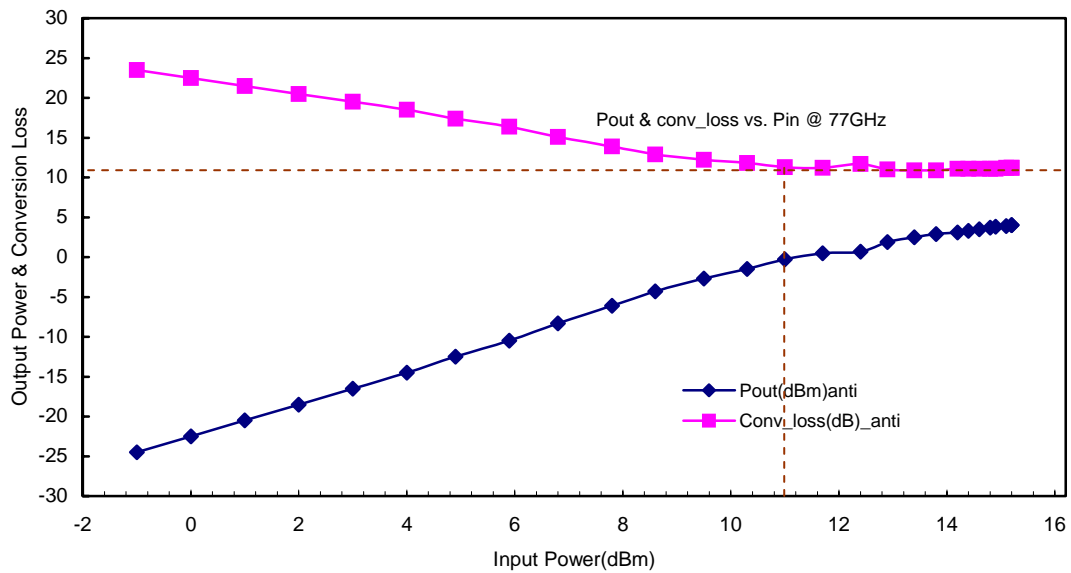
(a) Diodes in the reverse direction



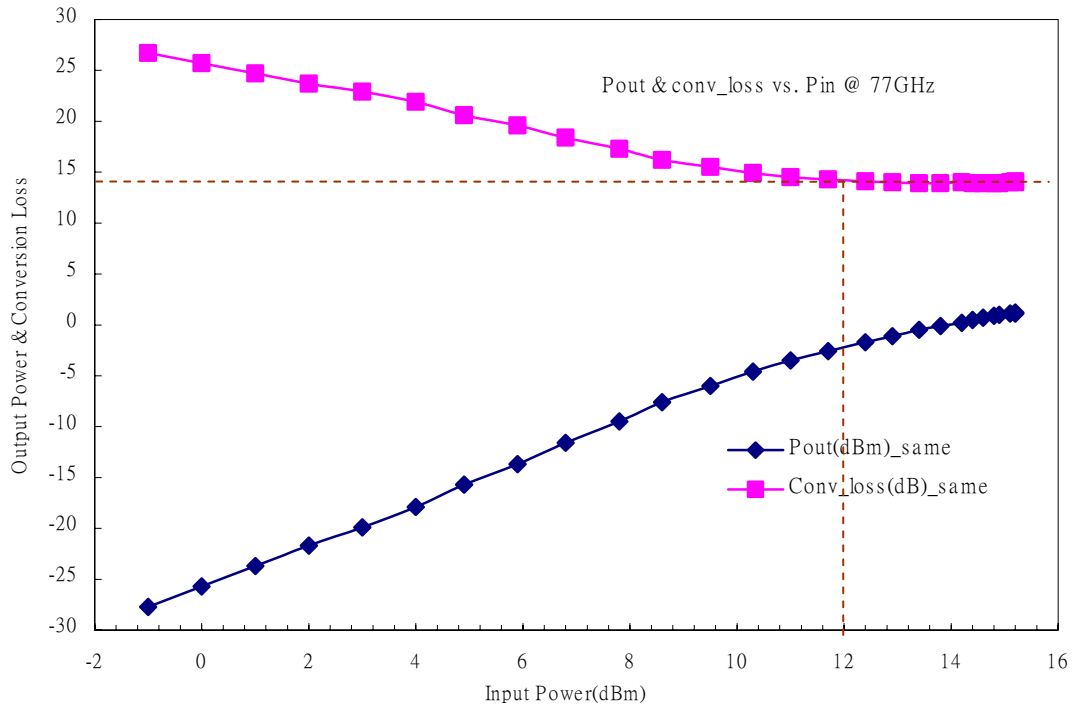
(b) Diodes in the same direction

Fig2.1-7 Measured conversion loss versus frequency of the rat-race ring doubler

Fig2.1-8(a) and (b) are measurements of conversion loss at 77GHz versus input power of the rat-race ring frequency doubler with diodes in reverse and same direction respectively.

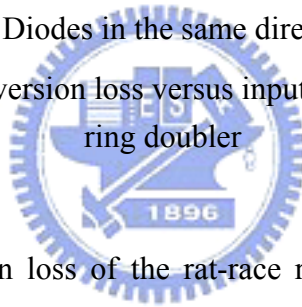


(a) Diodes in the reverse direction



(b) Diodes in the same direction

Fig2.1-8 Measurement of conversion loss versus input power at 77GHz of the rat-race ring doubler



The measured conversion loss of the rat-race ring doubler with diodes in the reverse direction shown in Fig2.1-7(a) is typically 12dB from 70GHz to 81.5GHz and less than 16dB up to 90GHz. Fig2.1-8(a) is the relationship of conversion loss versus power of fundamental frequency  $f_0$ . The conversion loss becomes better as the input power is getting larger. The doubler saturates when the input power reaches 11dBm. Meanwhile, the conversion loss is 11dB.

In the case of the rat-race ring doubler with diodes in the same direction, the conversion loss is around 15dB from 70GHz to 87GHz and still below 17dB up to 90GHz as shown in Fig2.1-7(b). The conversion loss is also getting better as the input power becomes larger as depicted in Fig2.1-8(b). The doubler saturates when the input power reaches 12dBm and the conversion loss is 14dB.

The rat-race ring doubler with diodes in reverse direction has better conversion loss than the one with diodes in the same diodes. This may mainly result from the practical imbalance of the rat-race ring. Check the balance of the sum port and delta port of the broad-band rat-race ring from section 3.4 of [6]. The thesis shows that both magnitude and phase imbalance of delta port is more severe. This is reasonable since the delta port contains a twisted line but the sum port doesn't. The measurements validate that the imbalance degrades the conversion loss. Hence, the doubler, which delivers fundamental signal to the sum port and obtain 2<sub>nd</sub> harmonic signal at the delta port, has better performance.

Fig 2.1-9 shows the conversion loss of the rat-race ring doubler with diodes in reverse direction in the whole band. The rat-race ring with an ideal phase inverter could operate in a broad bandwidth. Consequently, the rat-race ring doubler could also function in such a wide band as the figure shows. If we define 15dB as the boundary of the conversion loss, the doubler can handle from 25GHz to almost 90GHz.

Fig 2.1-10 is the isolation of the rat-race ring doubler with diodes in reverse direction in the whole band. The isolation is better than 30dB from 20GHz to 55GHz and at least 20dB in the whole band.

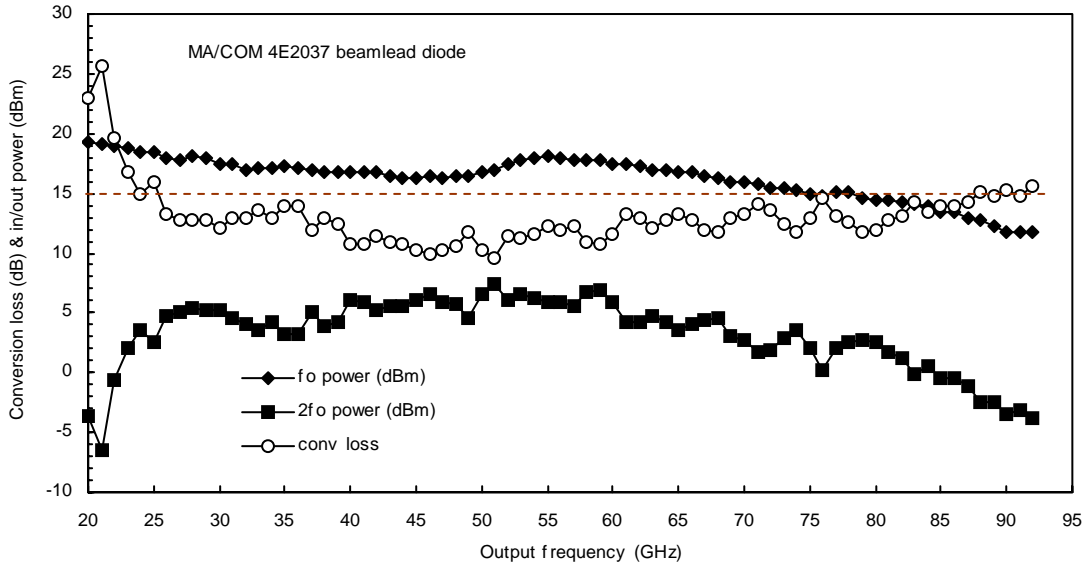


Fig2.1-9 Measured conversion loss of the rat-race ring doubler with diodes in the reverse direction in the whole band

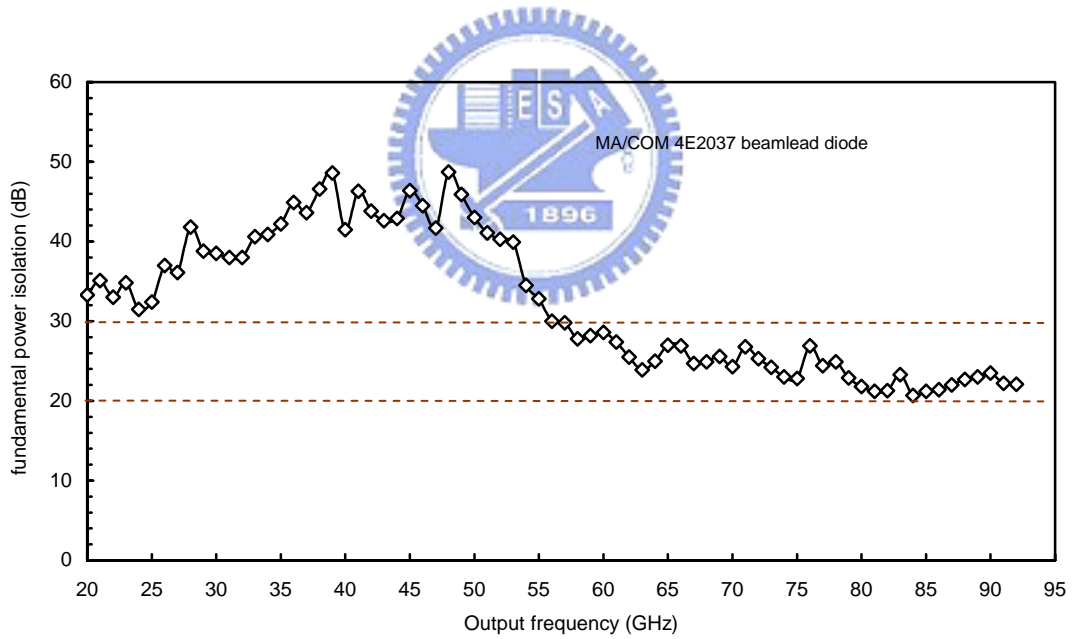


Fig2.1-10 Measured isolation of the rat-race ring doubler with diodes in the reverse direction in the whole band

## **Part II : Balun-type**

Balun is a transformer between balanced signal and unbalanced signal, which is widely utilized in balanced circuits, multipliers and antennas etc. In this part, two balun-type doublers are presented. The first one employs the coplanar waveguide (CPW) to coplanar stripline (CPS) transition as a broad-band balun. The balun is referred to [7]. The second one employs a broadband CPW balun, composed of an ideal phase inverter and a T-junction. The T junction is one CPW input and two CPS output. The CPW-balun type doubler is also published in [8]. Both two balun doublers are implemented on the same substrate as the rat-race ring doubler does.

### **2.2 CPW to CPS transition Balun-type frequency doubler**

#### **2.2.1 Circuit analysis**

The balun based on [7] has the layout as depicted in Fig2.2-1. The left side of this figure is CPS balanced port, and the right side is CPW unbalanced port. The line width and gap of CPW are 3mils and 1.5mils. The gap and the conductor width of the CPS port are 1mil and 10mils. Since a gap mismatch exit between CPS and CPW, the lower gap of the CPW has been tapered from 1mil to 1.5mils from left to right that eliminates the discontinuity.

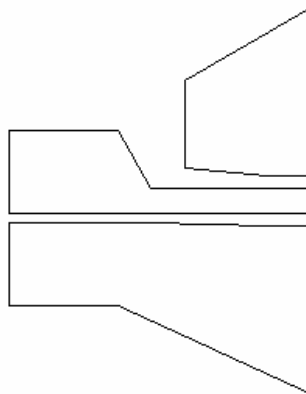


Fig2.2-1 Physical layout of CPW to CPS transition balun

Fig2.2-2 shows the measured results of two back-to-back connected baluns. The figure indicates both insertion loss and return loss of the balun. The insertion loss nearby 77GHz is roughly 2.5dB, and the return loss is better than 10dB up to 110GHz.

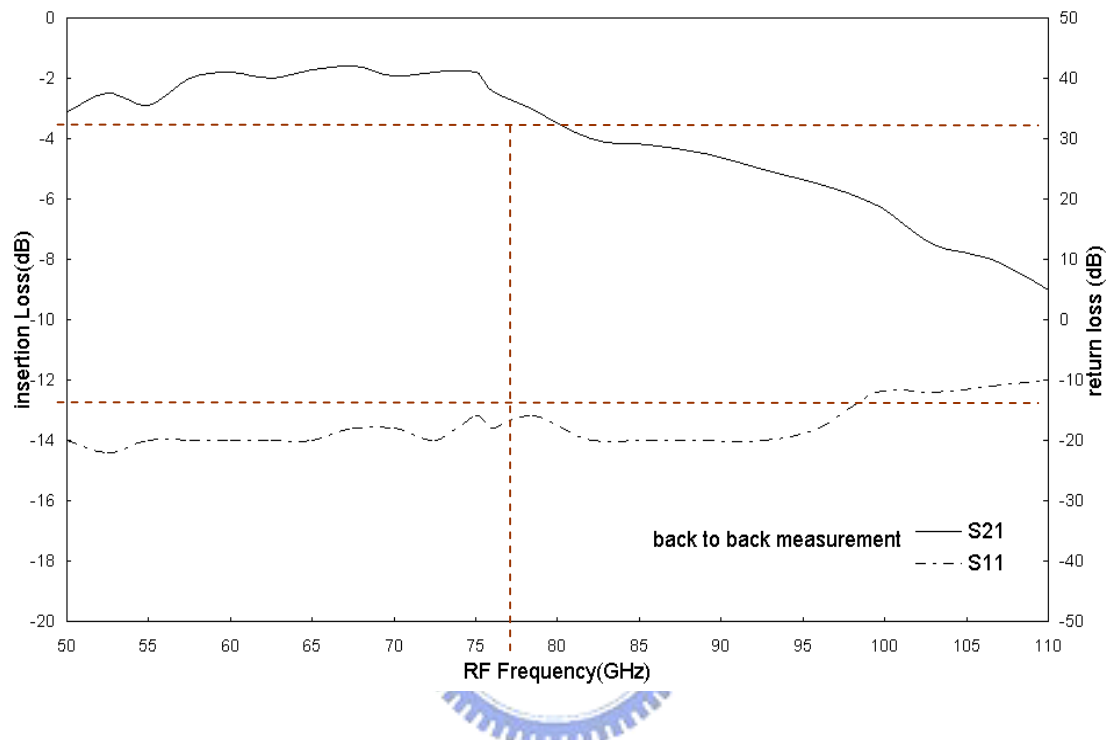


Fig2.2-2 The measurement of back-to-back connected CPW-CPS balun

The circuit model of balun is a transformer as shown in Fig2.2-3. This characteristic of balun makes itself capable of constructing a frequency doubler. Subsequently, the voltage and current relationship, based on the previous section and the circuit model of balun, will graphically illustrate the operation of the balun-type doubler.



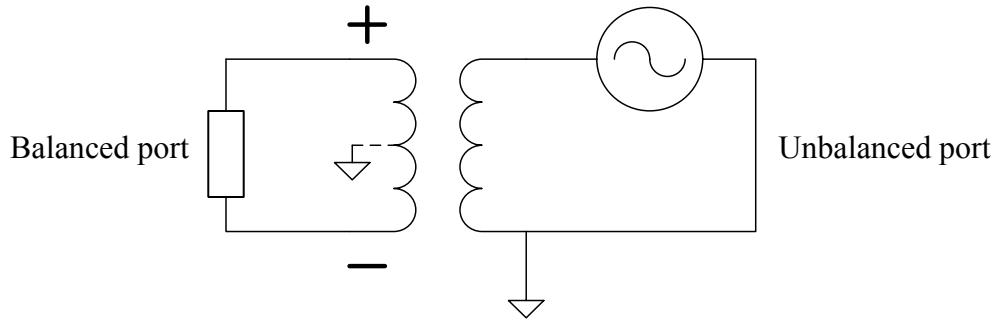


Fig2.2-3 Circuit model of balun

A balun-type doubler could be configured as Fig2.2-4 shows. The fundamental signal is feed through the input CPW port. The diodes, placed at the balanced CPS port of CPW-CPS balun, will be turned on in different half period in the time domain. The balun, acting as a transformer, picks up the 2<sup>nd</sup> harmonic term through the unbalanced CPW port in the right side.

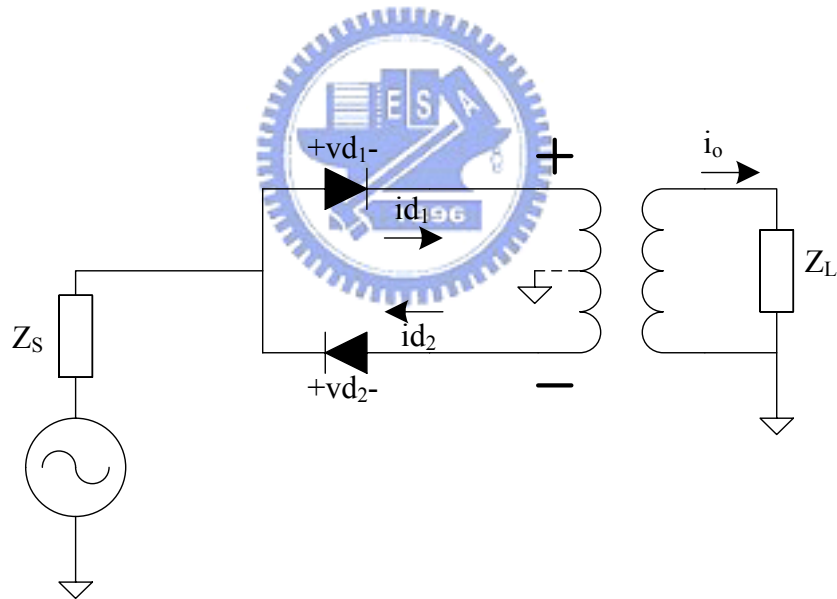


Fig2.2-4 Circuit model of balun-type doubler with diodes in the reverse direction

Fig2.2-5 is the voltage and current relationship based on the configuration of the circuit model in Fig2.2-4.  $v_{d1}$  equals  $v_{d2}$  but  $i_{d1}$  and  $i_{d2}$  conduct in different half period due to the reversed direction of forward bias of Schottky diodes. Hence,  $i_{d2}$  has a phase delay,  $\pi$ , relative to  $i_{d1}$ . Expand  $i_{d1}$  and  $i_{d2}$  into Fourier series form (2.3). We can find out that  $i_{d2} = i_{d1} * (-1)^n$ . The 2<sup>nd</sup> harmonic term would be  $i_{d2}^{(2)} = i_{d1}^{(2)}$ . Since

the transformer output current is  $i_o = id_1 + id_2$ , the  $2_{nd}$  harmonic term can be picked up by the transformer. On the other hand, because  $id_2^{(1)} = -id_1^{(1)}$ , the fundamental term won't appear at the output. If no transformer is located at the output, the output current will be  $i_o = id_1 - id_2$ . Therefore, the  $2_{nd}$  harmonic term will cancel out at the output. The circuit no longer behaves as a doubler.

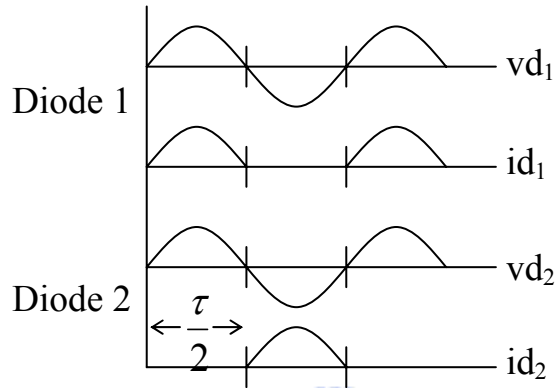


Fig2.2-5 Voltage and current relationship of balun-type doubler

$$\left. \begin{aligned}
 id_1 &= \sum g_n e^{jn\omega t} \\
 id_2 &= \sum g_n e^{jn\omega \left(t + \frac{\tau}{2}\right)} = \sum g_n e^{jn\omega t} e^{jn\pi} \\
 id_2^{(n)} &= id_1^{(n)} \cdot (-1)^n
 \end{aligned} \right\} (2.3)$$

The balun-type doubler could be modified in another configuration as shown in Fig2.2-6. The doubler can be fed through the right-side CPW port of CPW-CPS balun, and picks up the  $2_{nd}$  harmonic term in the left-side port (can be implemented merely by a CPW). When the doubler is configured in this way, the Schottky diodes must be placed in the same direction. Otherwise the  $2_{nd}$  harmonic term will disappear at the output. Fig2.2-7 shows the voltage and current relationship of balun-type balun with diodes in the same direction.

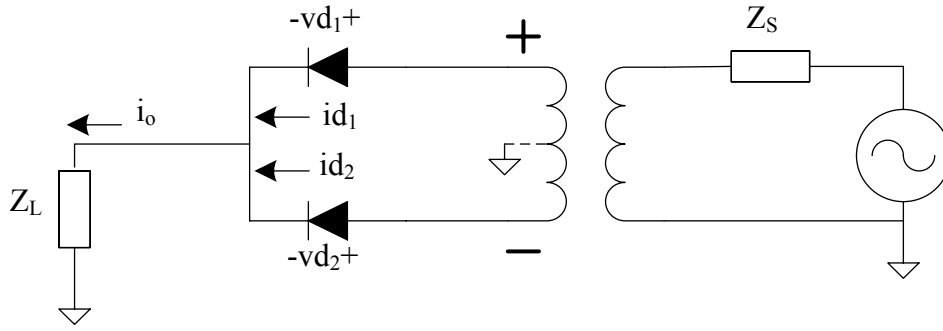


Fig2.2-6 Circuit model of balun-type doubler with diodes in the same direction

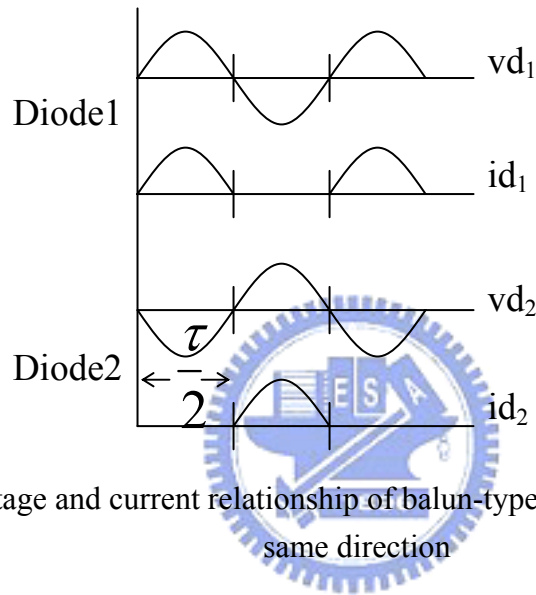


Fig2.2-7 Voltage and current relationship of balun-type doubler with diodes in the same direction

The fundamental signal feeds to CPW port of the balun and becomes balanced signal. The voltages across the Schottky diodes,  $vd_1$  and  $vd_2$ , consequently differ from each other with a half period in the time domain. Expand the currents into Fourier series (2.4), deriving that  $id_2 = id_1 * (-1)^n$ . This relation results in that  $id_2^{(2)} = id_1^{(2)}$  and  $id_2^{(1)} = -id_1^{(1)}$ . The output current,  $i_o = id_1 + id_2$ , picks up the 2nd harmonic term and eliminates the fundamental one. Fig2.2-11 represents the measured conversion loss of the balun-type doubler with diodes in the same direction.

$$\left. \begin{aligned}
 id_1 &= \sum g_n e^{jn\omega t} \\
 id_2 &= \sum g_n e^{jn\omega \left(t + \frac{\tau}{2}\right)} = \sum g_n e^{jn\omega t} e^{jn\pi} \\
 id_2^{(n)} &= id_1^{(n)} \cdot (-1)^n
 \end{aligned} \right\} (2.4)$$

### 2.2.2 Circuit implementation and measurement

The CPW-CPS balun doubler with diodes in the same direction is fabricated as Fig2.2-8. Fig2.2-9 indicates the measured conversion loss of the balun-type doubler. The conversion loss is around 22.5dB from 72GHz to 90GHz.

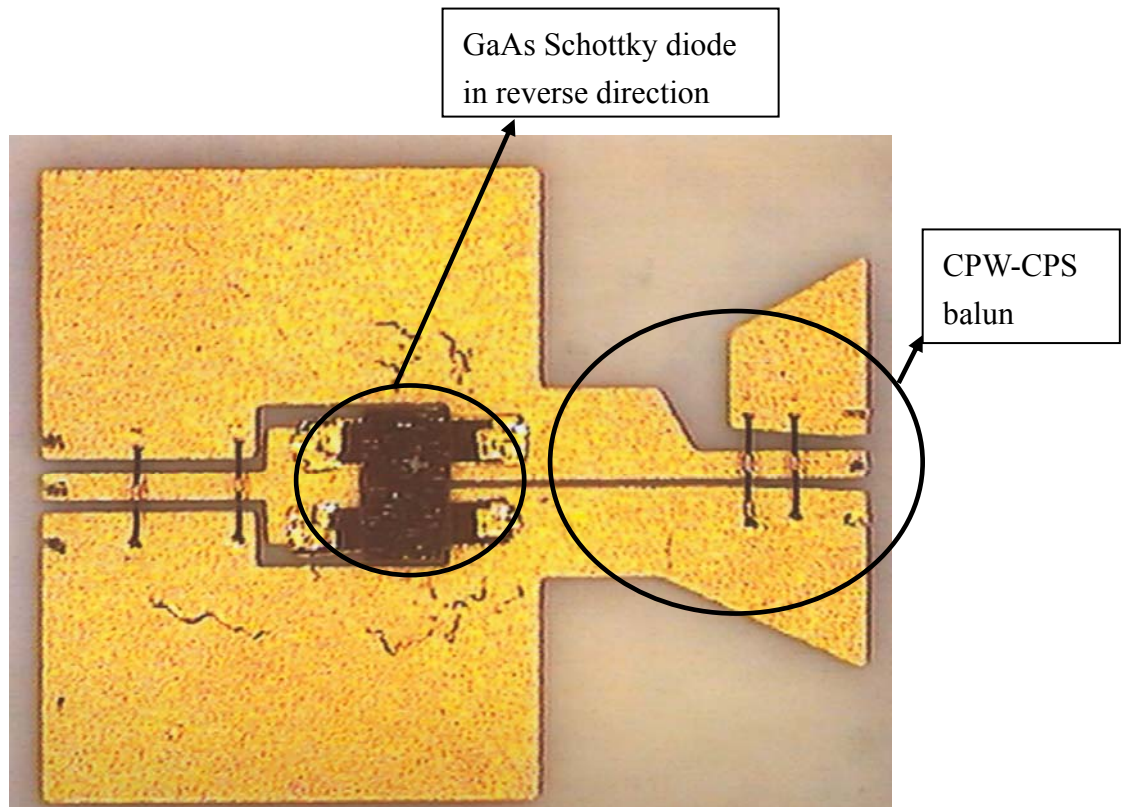


Fig2.2-8 Balun-type doubler layout with diodes configured in the reverse direction

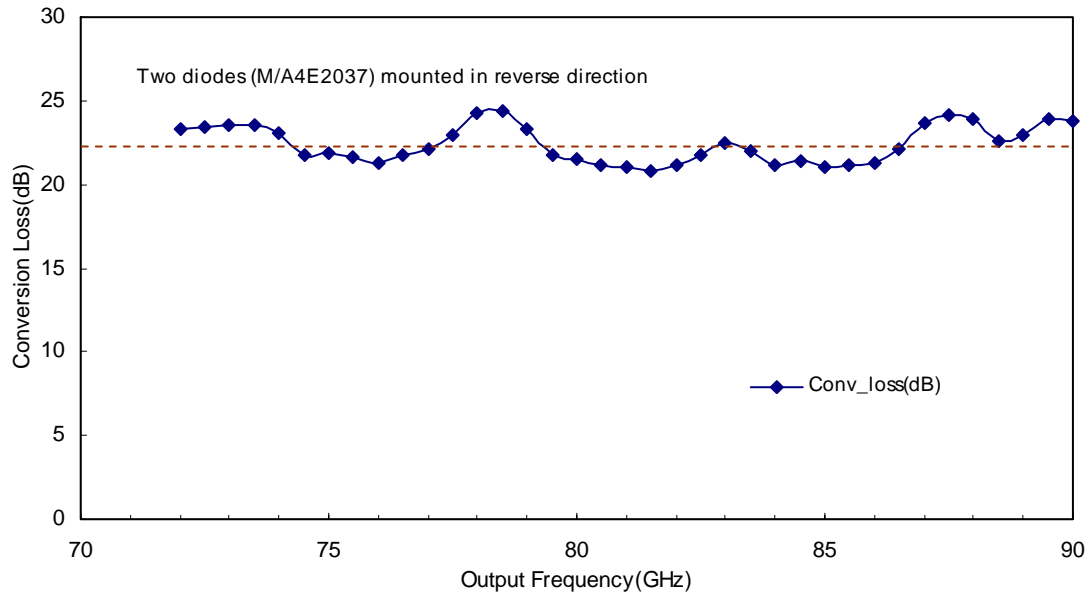


Fig2.2-9 Measured conversion loss of balun-type doubler with diodes in reverse direction

The CPW-CPS balun doubler with diodes in the same direction is fabricated as shown in Fig2.2-10. Fig2.2-11 indicates the measured conversion loss of the balun-type doubler with diodes in the same direction. The conversion loss is around 22.5dB from 72GHz to 90GHz.

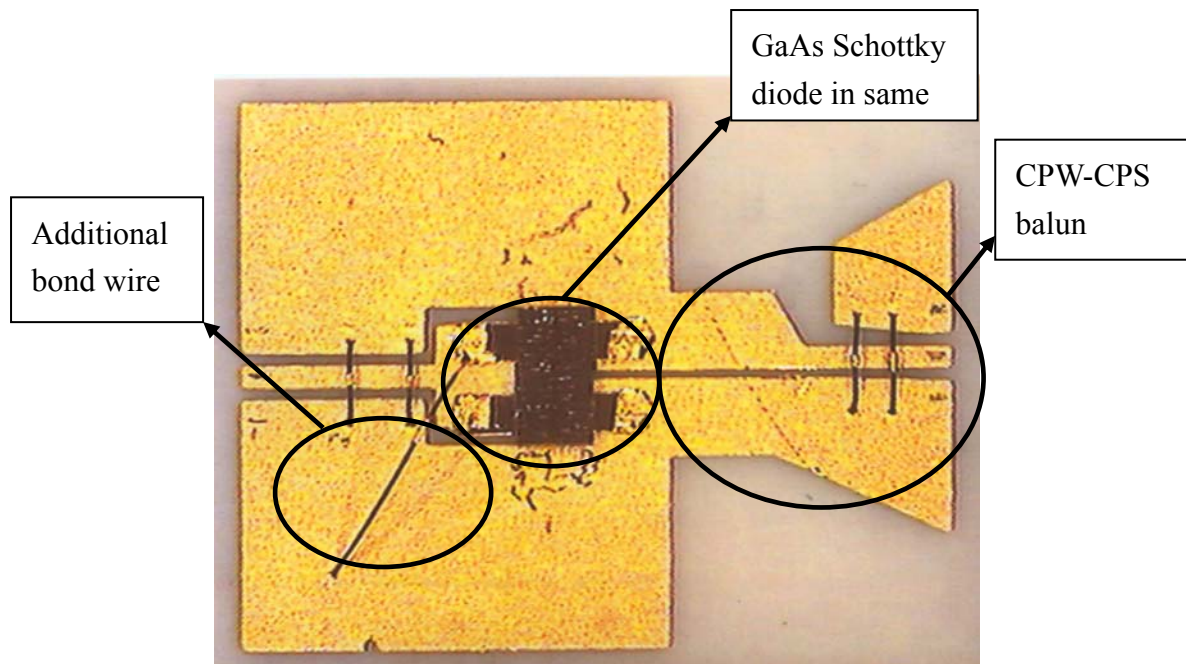


Fig2.2-10 Balun-type doubler layout with diodes configured in the same direction

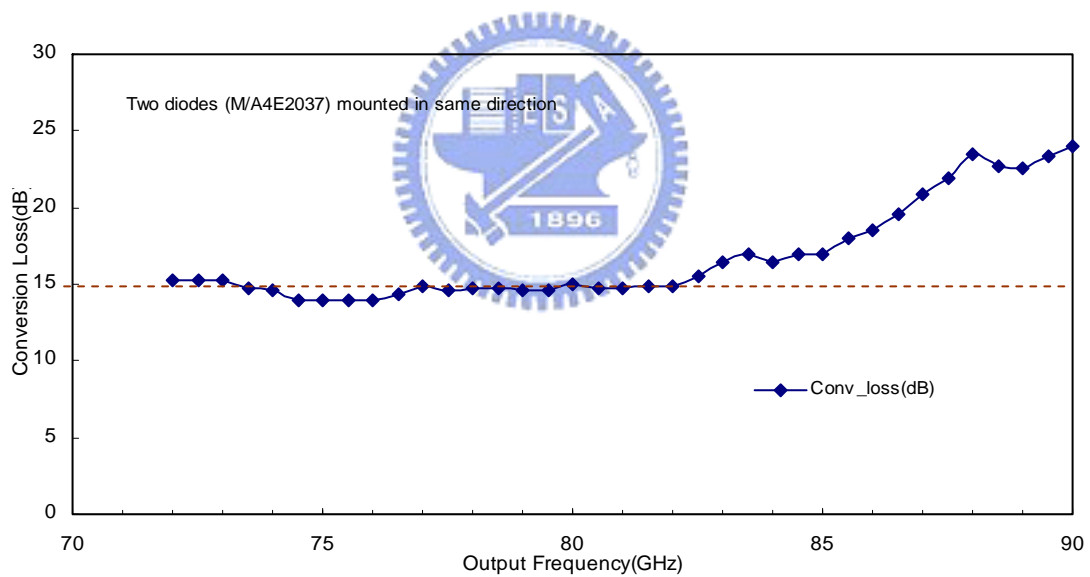
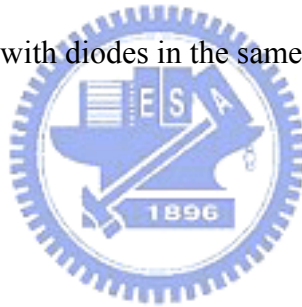


Fig2.2-11 The measured conversion loss of balun-type doubler with diodes in the same direction

The circuit size of the CPW-CPS balun doubler is 70mil x 91mil. The conversion loss of balun-type doubler with diodes in the same direction is 15dB from 72GHz to 82GHz and getting worse above 82GHz. The conversion loss of balun-type doubler with diodes in the same direction is at least 7.5dB better than that of the diodes in the reverse direction. This is due to the signal at  $2f_0$  frequency passing through the balun.

When the diodes are configured in the reverse direction, the signal passing through the balun is at 2<sup>nd</sup> harmonic frequency and the balun at  $2f_0$  has larger loss. In the same direction configuration, the signal passing the balun is at the fundamental frequency and the balun at  $f_0$  has much less loss. As a result, the reverse direction configuration would have larger loss which leads to worse conversion loss. Notably, an additional long bond wire is required for discharging the accumulated charge, resulting from the same direction of diode currents as shown in Fig2.2-10. The long bond wire has high reactance for RF signal, thus preventing RF signal from going through it. Fig2.2-12 shows the relationship of conversion loss versus input power at 77GHz. The conversion loss saturates as the input power is about 15dBm for both reverse and same direction configurations. Fig2.2-13 depicts the broadband measurement of conversion loss of CPW-CPS balun type doubler with diodes in the same direction.



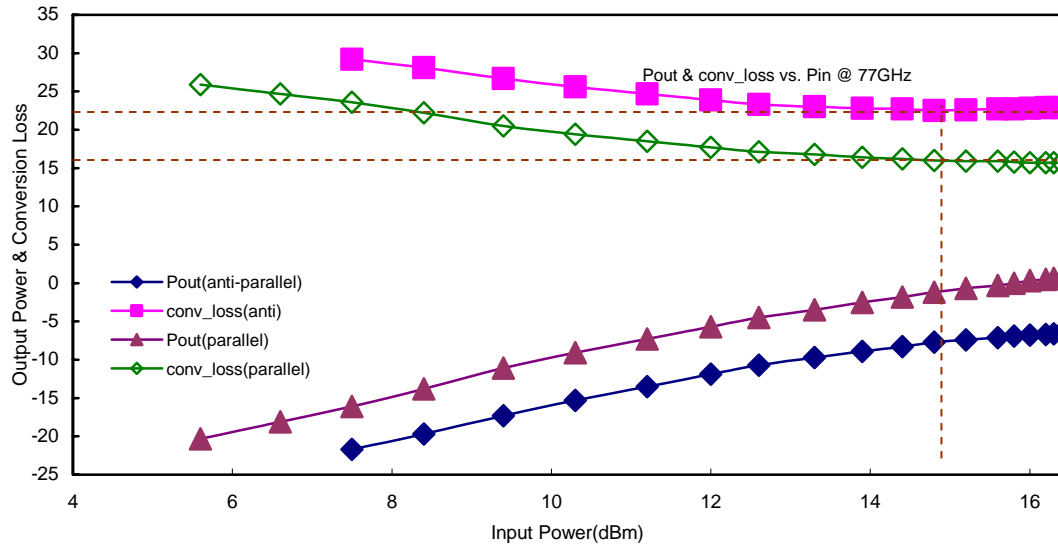


Fig2.2-12 Measurement of conversion loss versus input power at 77GHz of the CPW-CPS balun doubler

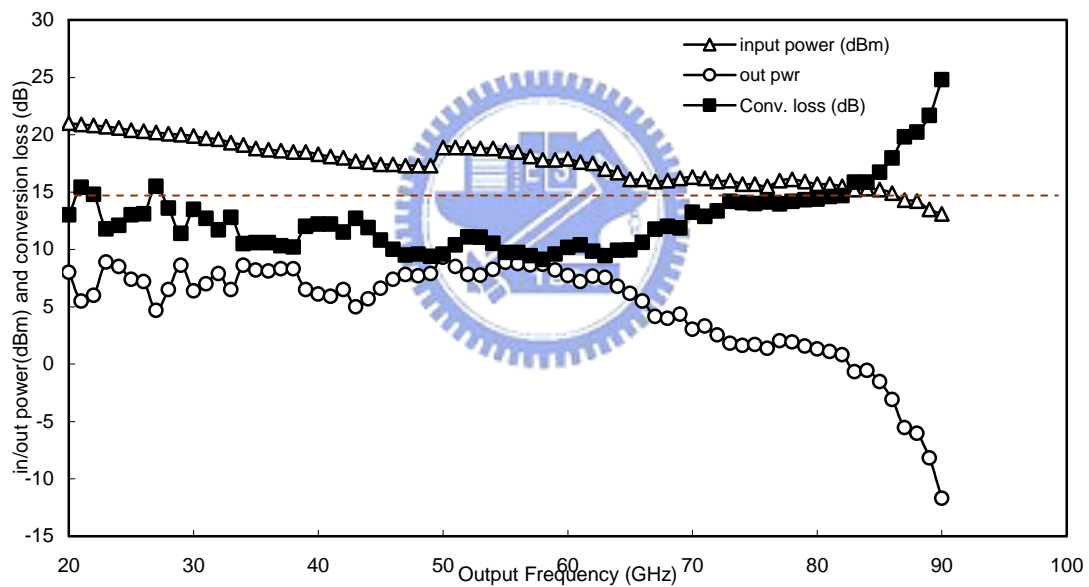


Fig2.2-13 Broadband measurement of conversion loss of CPW-CPS balun type doubler with diodes in the same direction



## 2.3 Broadband CPW balun-type doubler

### 2.3.1 Circuit analysis

The circuit schematic is illustrated in Fig2.3-1. The doubler consists of a CPW-CPW T junction and two CPS-to-CPW transition. The input signal,  $f_o$ , is divided into two out-of-phase signals at the output. The phase inversion is achieved by these two CPS-to-CPW transitions. Figure 2.3-2 explains the phase inversion. The CPW balun has broadband performance.

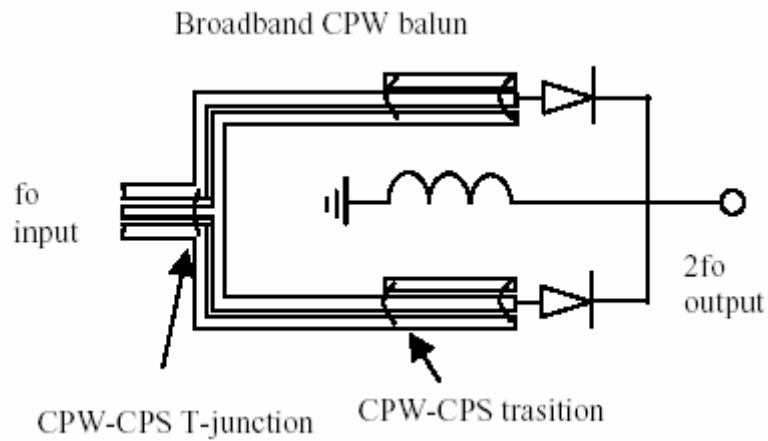


Fig2.3-1 The schematic of the CPW balun-type doubler

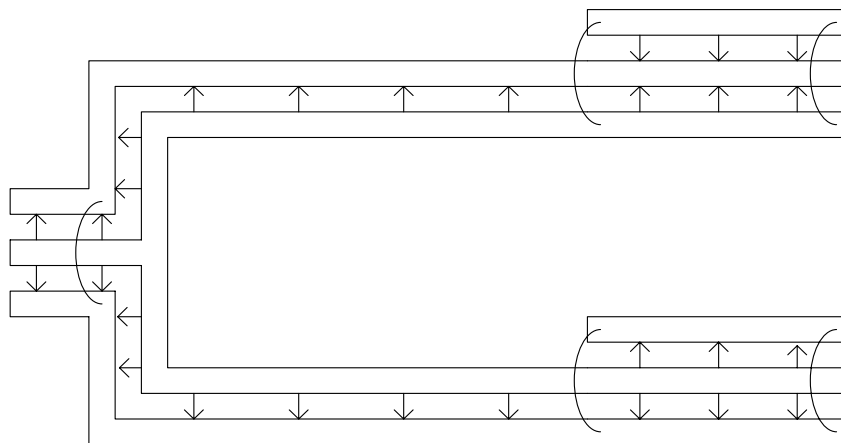
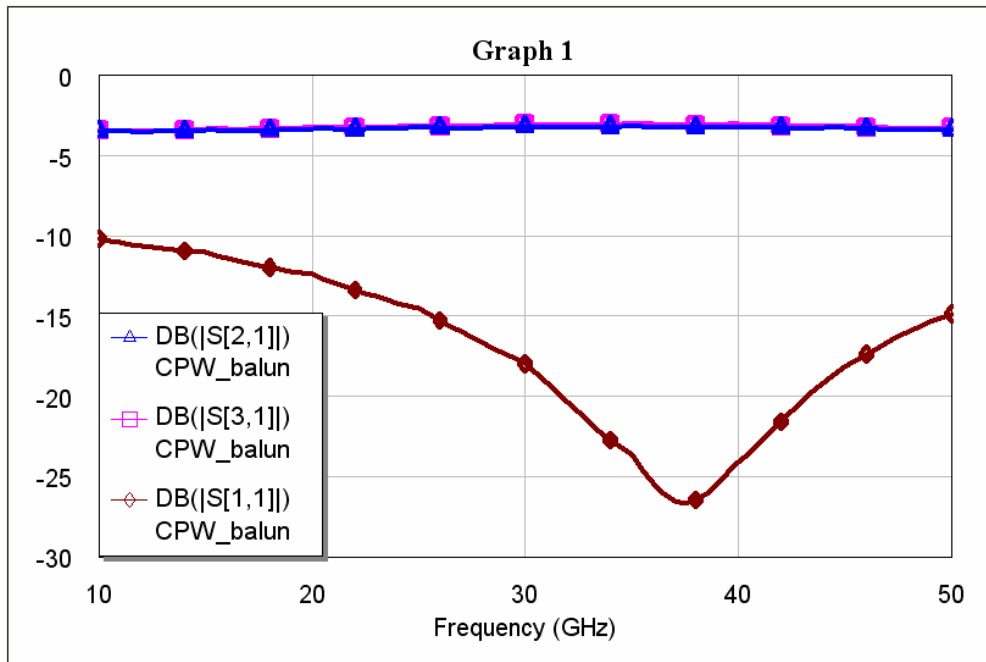
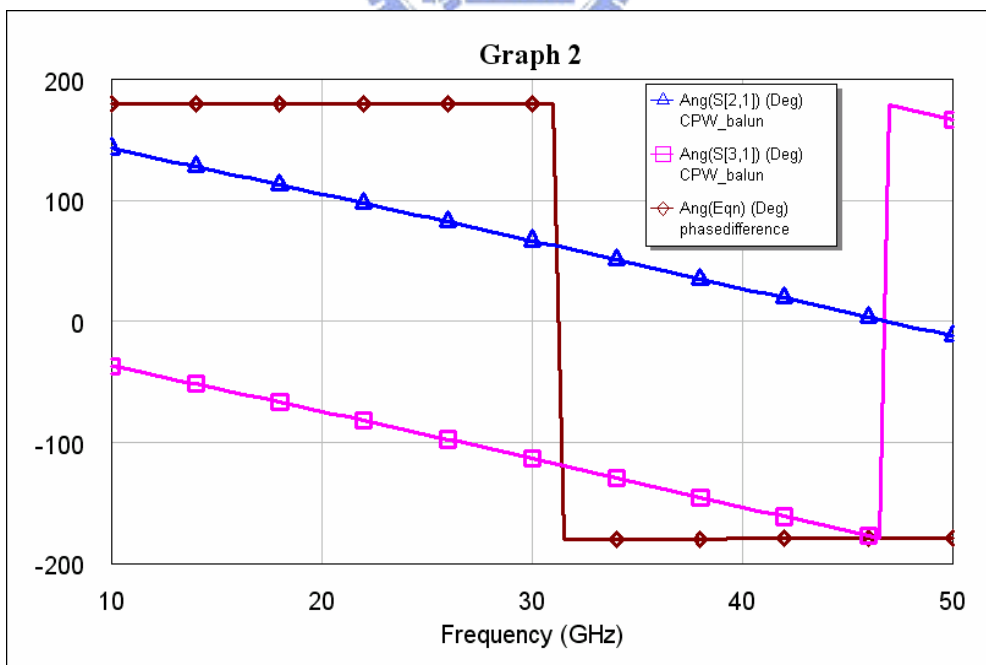


Fig2.3-2 E-field distribution of CPW balun

The CPS lines of the CPW balun are designed with characteristic impedance of  $70.7\Omega$  and length of quarter wavelength at 38.5GHz. The simulated performance of the balun is depicted in Fig2.3-3.



(a) Simulated magnitude response of CPW balun



(b) Simulated phase response of CPW balun

Fig2.3-3 Simulated result of CPW balun

The simulation of CPW balun shows that it indeed performs well in a broad bandwidth. The following task is to configure the CPW balun as a frequency doubler. Like previous balun-type doubler, the CPW balun-type doubler can be configured by feeding  $f_0$  to the unbalanced port and connecting two diodes in the same direction. Fig2.3-5 depicts the circuit model of the CPW balun doubler. Based on this circuit model, the voltage and current of the diodes would have the relationship as Fig2.3-6 shows.

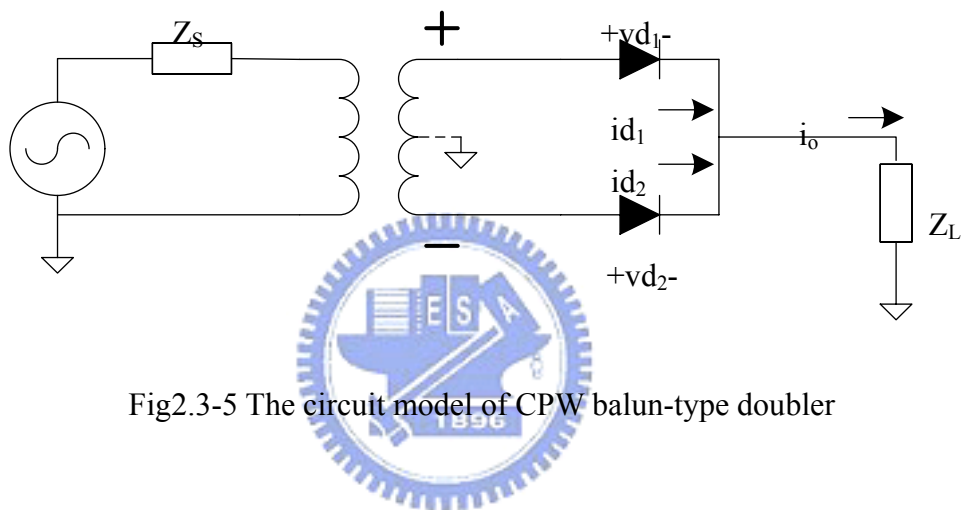


Fig2.3-5 The circuit model of CPW balun-type doubler

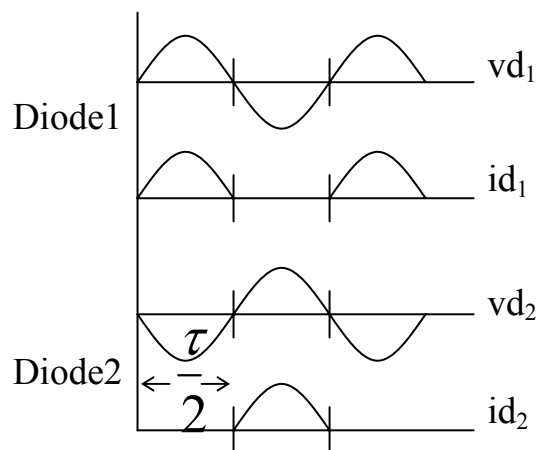


Fig2.3-6 The voltage and current relationship of CPW balun-type doubler

The fundamental signal is applied to input CPW port of T junction of the balun.  $v_{d1}$  and  $v_{d2}$ , the voltages across the Schottky diodes, therefore differ from each other with a half period in the time domain due to the ideal phase inverter. Expand the currents of two diodes into Fourier series (2.4), deriving that  $i_{d2} = i_{d1} \cdot (-1)^n$ . This relation brings about that  $i_{d2}^{(2)} = i_{d1}^{(2)}$  and  $i_{d2}^{(1)} = -i_{d1}^{(1)}$ . The output current,  $i_o = i_{d1} + i_{d2}$ , sums the 2nd harmonic term and eliminates the fundamental one.

$$\left. \begin{aligned} i_{d1} &= \sum g_n e^{jn\omega t} \\ i_{d2} &= \sum g_n e^{jn\omega \left(t + \frac{\tau}{2}\right)} = \sum g_n e^{jn\omega t} e^{jn\pi} \\ i_{d2}^{(n)} &= i_{d1}^{(n)} \cdot (-1)^n \end{aligned} \right\} (2.5)$$

### 2.3.2 Circuit implementation and measurement

Fig2.3-7 and Fig2.3-8 are the physical layout and measured response of the CPW balun doubler respectively. The circuit size is 100mil x 66mil.

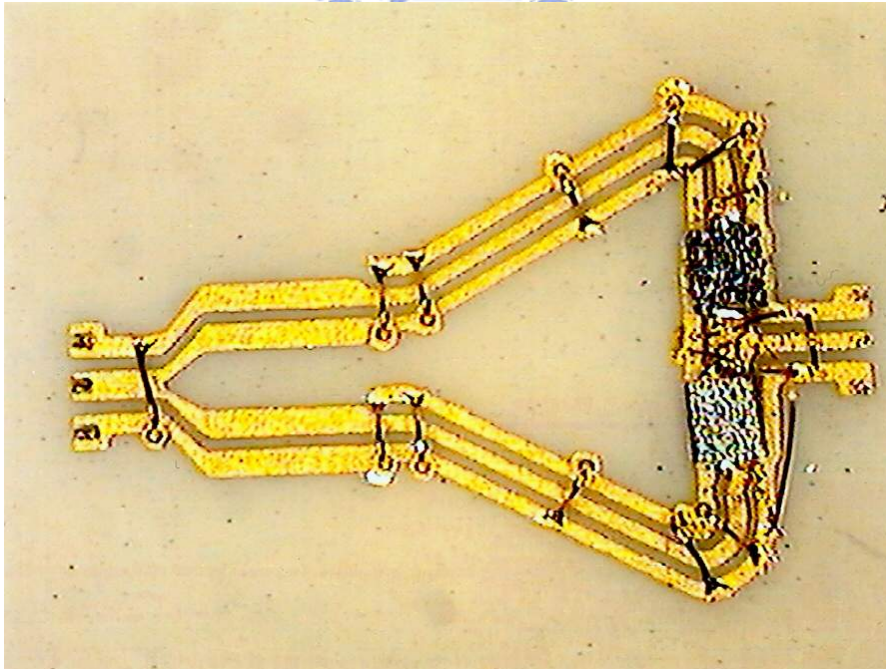
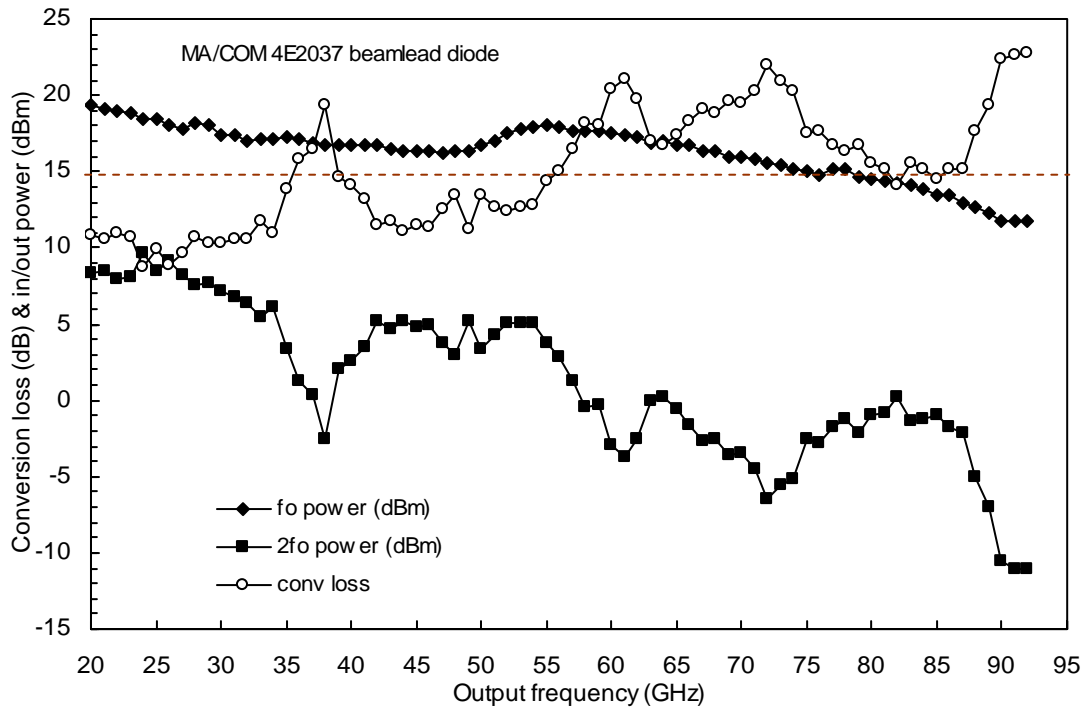
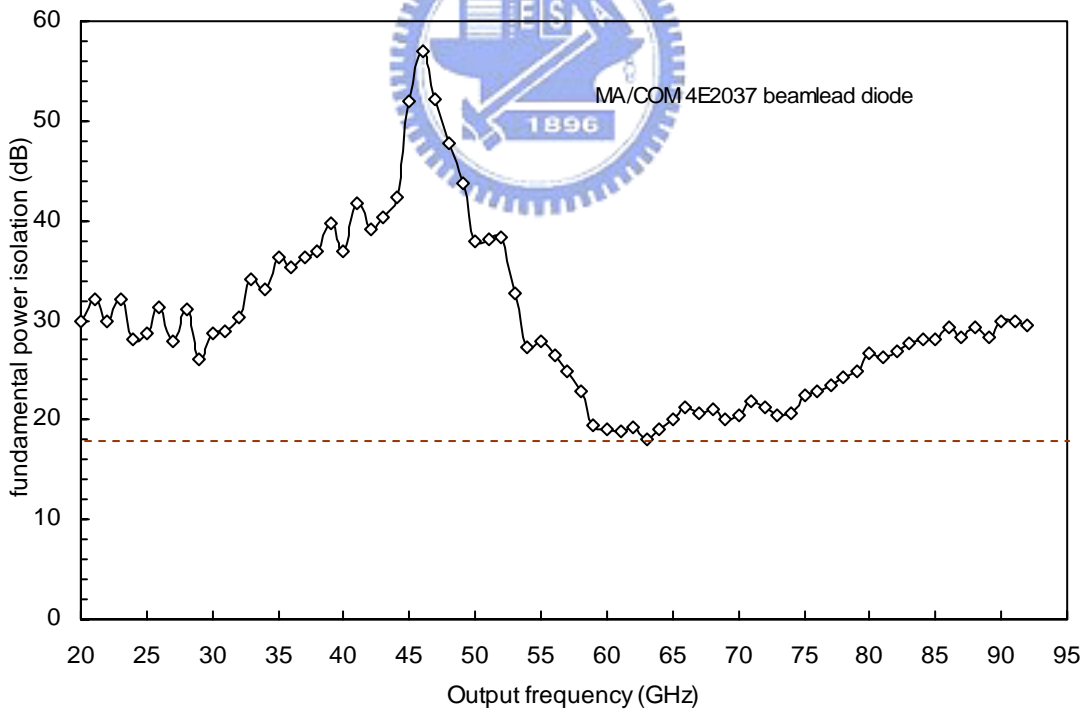


Fig2.3-7 Physical layout of CPW balun-type doubler



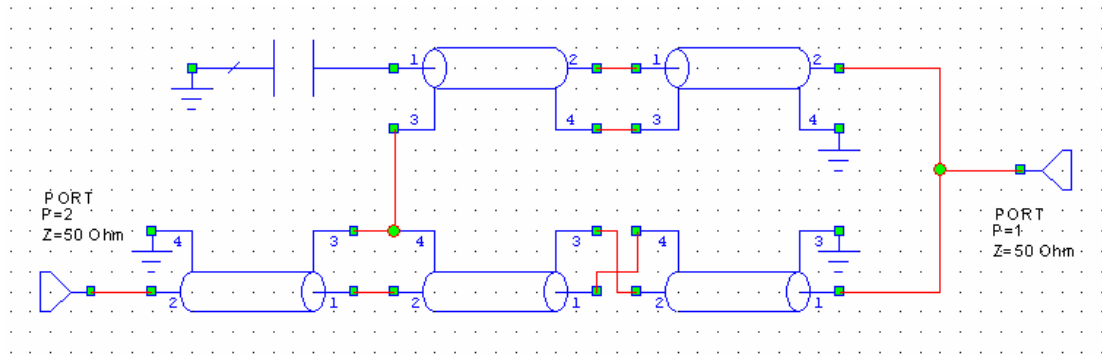
(a) Broad band measurement of conversion loss response



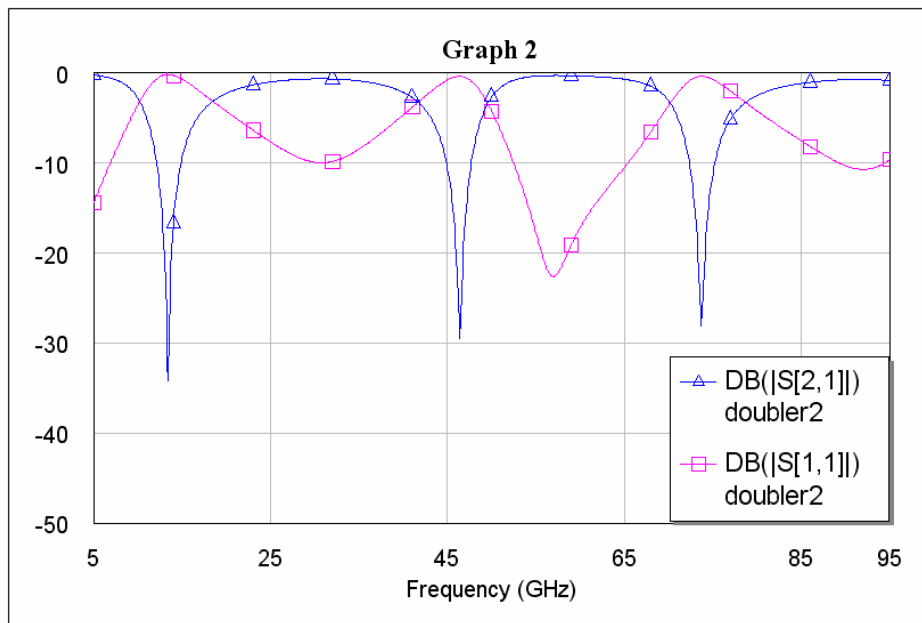
(b) Broad band measurement of isolation response

Fig2.3-8 Measurement of CPW balun-type doubler

The conversion loss is typically 11dB from 20 to 34GHz, 13dB from 40 to 56GHz, 16dB from 75 to 81GHz. Some resonances occur around frequencies of 38, 62, 72, and 93GHz. The measured isolation is at least 20dB in the whole band except few frequencies. The resonant phenomenon happens due to several possible reasons. First, although the simulated result of the CPW balun alone without diodes shows good performance in broad bandwidth, the termination of the CPW balun-type doubler is diode, not  $50\Omega$ . When the diode is reversed biased, the balun sees a capacitor at the termination. This non- $50\Omega$  termination will reflect the signal back to the T junction and cause resonance. Fig2.3-9 is the simulated resonance.



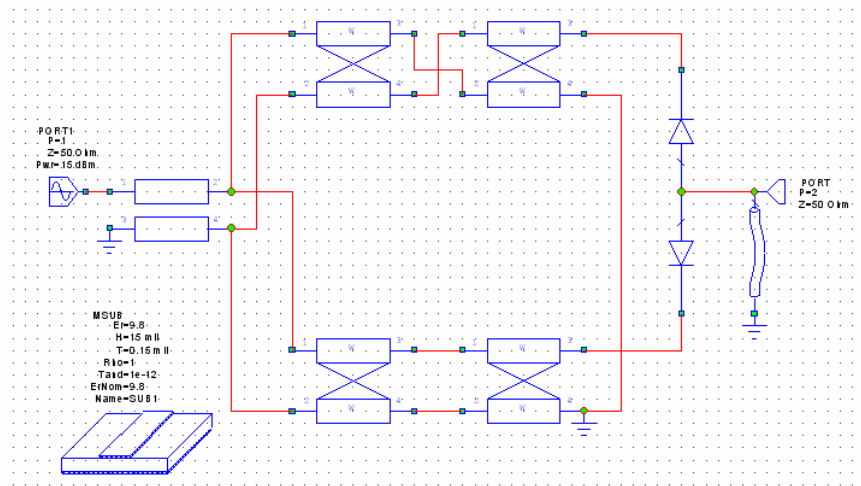
(a) Circuit model of doubler resonance



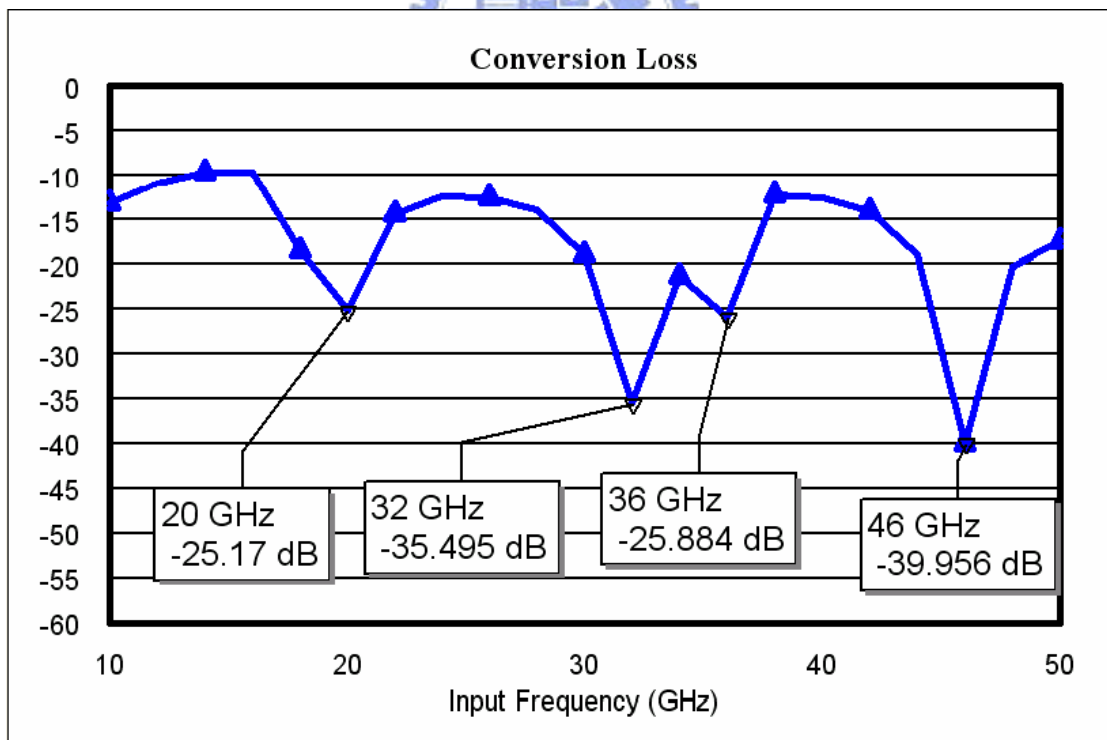
(b) Simulated response of resonance

Fig2.3-9 Simulation of doubler resonance

Second, a loop, resulted from the twisted line, would also form resonance. Third, the parasitic inductor of bond wire and the effect of the CPW bend implemented in the physical layout would degrade the performance and even resonate. The overall effect is simulated in Fig2.3-10 to demonstrate the resonance.



(a) Circuit model of doubler including parasitic effect



(b) Simulated conversion of CPW balun-type doubler including parasitic effect

Fig2.3-10 Non-linear simulation of CPW balun doubler including bond wire parasitic effect and twisted line

# Chapter 3 Switch

Switches, which direct the signal or power flow, are extensively used in radars, instruments, antennas, and communication systems etc. When switch is discussed, several issues about it are concerned such as bandwidth, switching speed, power handling, high isolation, low voltage operations, and high operating frequency. Two kinds of semiconductor devices can be used for switches: transistors and diodes. A PIN diode switch has lower loss and handles high power levels. A MESFET switch consumes negligible power and has very fast switching speed. A MESFET switch can even provide possible power gain if the transistor is worked in active mode.

## 3.1 Theory of Switch design

The performance of a practical switch can be expressed by specifying its insertion loss and isolation as the basic design parameters [10].

**Insertion loss:** It is defined as the ratio of the power delivered to the load in the “ON” state of the ideal switch to the actual power delivered by the practical switch. It is usually expressed in decibels and is a positive number.

**Isolation:** It is defined as the ratio of the power delivered to the load for an ideal switch in the ON state to the actual power delivered to the load then the switch is in the “OFF” state. This is also expressed in decibels and is a positive quantity.

When the switch is in ON state, the signal should be able to pass through the switch. Insertion loss measures the loss as the signal penetrates through it. When the switch is in OFF state, the signal should not be able to pass through the switch. Isolation measures the ability about how the switch blocks the signal.



There are several types of switches are used most frequently in microwave frequencies as Fig3.1 depicts. They are single-pole-single-through (SPST), single-pole-double-through (SPDT), and single-pole-triple-through (SP3T) etc. The switch controls which path the signal goes through. Besides, the switches are further classified into two categories: reflective and non-reflective. In reflective switch, the signal is reflected to the source terminal at OFF state. This causes significant standing waves between components which might be a problem in some applications. In non-reflective switch, the signal would be absorbed in excess path and termination. Thus, more devices and  $50\Omega$  terminations should be added into the circuit. Fig3.2 represents the examples of reflective and non-reflective switches in SPST configuration. The designed W-band SPST and SPDT adopts reflective switch.

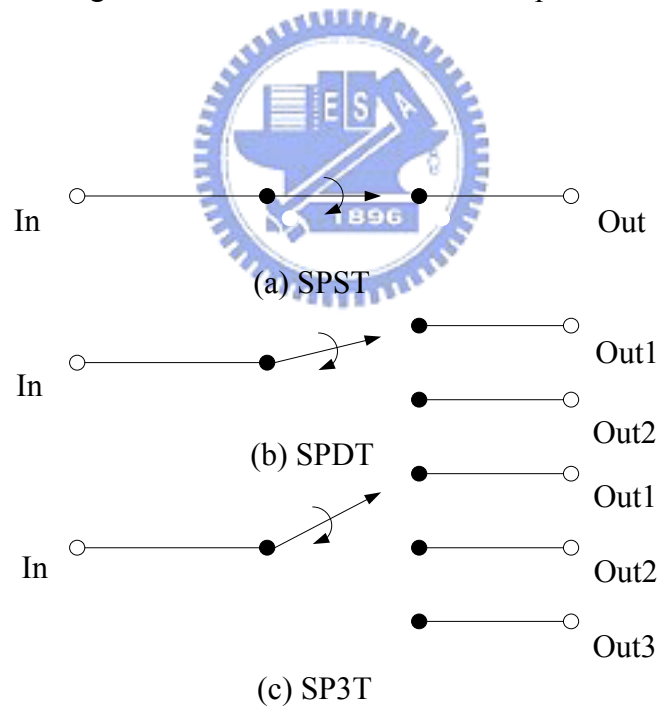


Fig3-1 Switch configuration

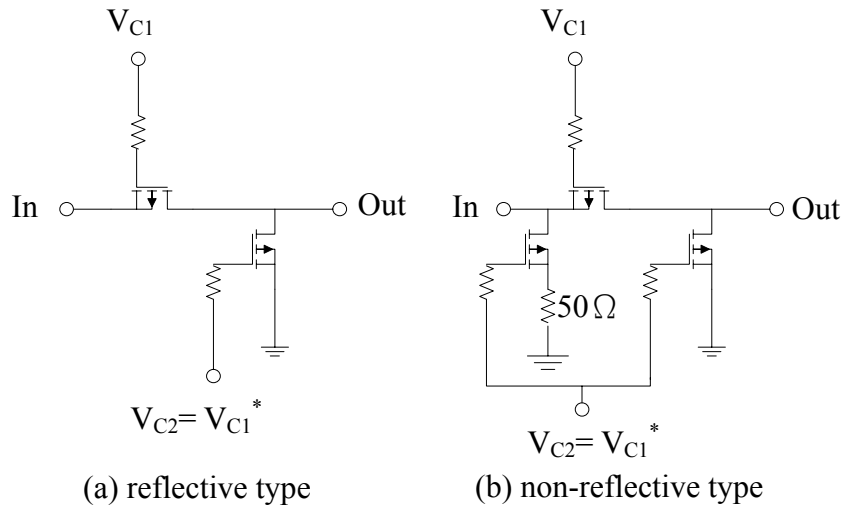


Fig3-2 Two classifications of switches

Moreover, there are three types of reflective SPDT switch configurations as shown in Fig3-3. They are series, shunt, and series-shunt configurations separately.

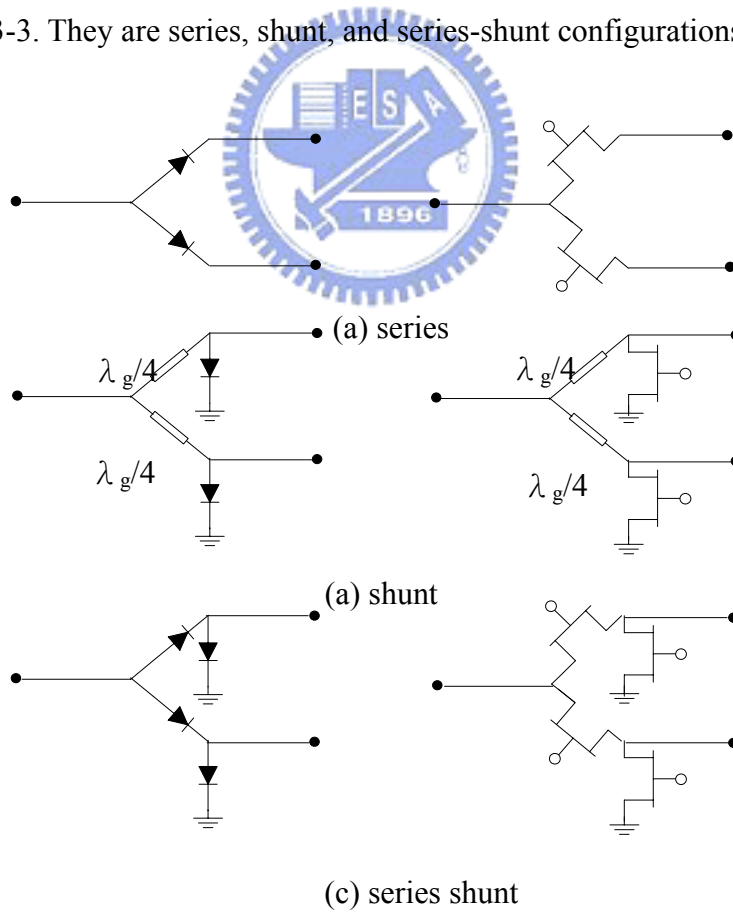
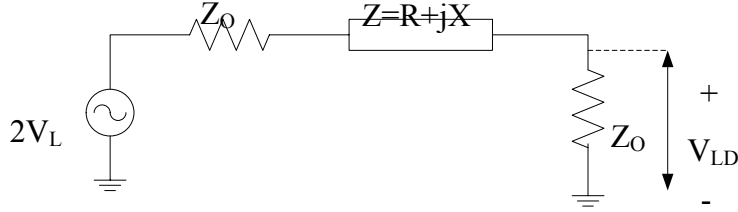


Fig3.3 Reflective switch configurations for SPDT

From above configuration and circuit theory, it's already enough to derive individual insertion loss and isolation. For simplicity, the derivation is based on SPST.

(a) Series configuration

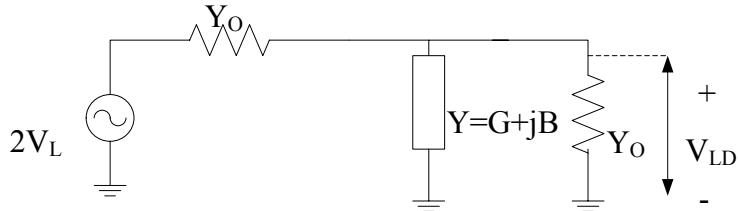


$$P_{ideal} = \frac{1}{Z_o} \left( \frac{Z_o}{Z_o + Z_o} \cdot 2V_L \right)^2 = \frac{V_L^2}{Z_o}$$

$$P_{actual} = \frac{V_{LD}^2}{Z_o} = \frac{1}{Z_o} \left( \frac{Z_o}{Z_o + Z + Z_o} \cdot 2V_L \right)^2 = \left( \frac{2V_L}{Z_o \cdot (2Z_o + Z)} \right)^2$$

$$\begin{aligned} \mathbf{Iso}_{series} = \mathbf{IL}_{series} &= \left| \frac{P_{ideal}}{P_{actual}} \right| = \left| \frac{V_L^2}{Z_o} \cdot \left( \frac{Z_o \cdot (2Z_o + Z)}{2V_L} \right)^2 \right| = \left| \frac{2Z_o + Z}{2Z_o} \right|^2 \\ &= \left| 1 + \left( \frac{Z}{2Z_o} \right) \right|^2 = \left| 1 + \frac{R}{2Z_o} + j \frac{X}{2Z_o} \right|^2 \\ &= 1 + \frac{R}{Z_o} + \frac{1}{4} \cdot \left( \frac{R}{Z_o} \right)^2 + \frac{1}{4} \cdot \left( \frac{X}{Z_o} \right)^2 \end{aligned} \quad (3.1)$$

(b) Shunt configuration



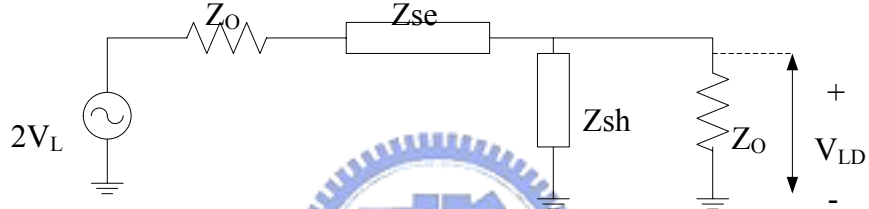
$$P_{ideal} = Y_o \cdot V_L^2$$

$$P_{actual} = Y_o \cdot V_{LD}^2 = Y_o \left( \frac{1}{\frac{Y + Y_o}{Y_o} + \frac{1}{Y + Y_o}} \cdot 2V_L \right)^2 = Y_o \left( \frac{Y_o \cdot 2V_L}{2Y_o + Y} \right)^2$$

$$\mathbf{ISO}_{shunt} = \mathbf{II}_{shunt} = \left| \frac{P_{ideal}}{P_{actual}} \right| = \left| \frac{Y_o \cdot V_L^2}{Y_o \left( \frac{Y_o \cdot 2V_L}{2Y_o + Y} \right)^2} \right| = \left| \frac{2Y_o + Y}{2Y_o} \right|^2 = \left| 1 + \left( \frac{Y}{2Y_o} \right) \right|^2 \quad (3.2)$$

$$= \left| 1 + \frac{G}{2Y_o} + j \frac{B}{2Y_o} \right|^2 = 1 + \frac{G}{Y_o} + \frac{1}{4} \cdot \left( \frac{G}{Y_o} \right)^2 + \frac{1}{4} \cdot \left( \frac{B}{Y_o} \right)^2$$

(c) Series-shunt configuration



$$P_{ideal} = \frac{1}{Z_o} \left( \frac{Z_o}{Z_o + Z_o} \cdot 2V_L \right)^2 = \frac{V_L^2}{Z_o}$$

$$P_{actual} = \frac{V_{LD}^2}{Z_o} = \frac{1}{Z_o} \left( \frac{Z_{sh} \parallel Z_o}{Z_o + Z_{se} + Z_{sh} \parallel Z_o} \cdot 2V_L \right)^2$$

$$\mathbf{II}_{series} = \mathbf{ISO}_{series} = \left| \frac{P_{ideal}}{P_{actual}} \right| = \left| \frac{V_L^2}{V_{LD}^2} \right| = \left| \frac{1}{\frac{2Z_{sh} \parallel Z_o}{Z_o + Z_{se} + Z_{sh} \parallel Z_o}} \right|^2 = \left| \frac{Z_o + Z_{se} + Z_{sh} \parallel Z_o}{2Z_{sh} \parallel Z_o} \right|^2$$

$$= \left| \frac{Z_o + Z_{se} + \frac{Z_{sh} Z_o}{Z_{sh} + Z_o}}{\frac{2Z_{sh} Z_o}{Z_{sh} + Z_o}} \right|^2 = \left| \frac{(Z_{sh} + Z_o)(Z_o + Z_{se}) + Z_{sh} Z_o}{2Z_{sh} Z_o} \right|^2$$

$$= \left| \frac{1}{2} + \frac{(Z_{sh} + Z_o)(Z_o + Z_{se})}{2Z_{sh} Z_o} \right|^2 \quad (3.3)$$

The derivation of insertion loss and isolation has been done for three types of reflective switch. It looks somewhat strange that the formulas for insertion loss and isolation are the same equations. This is natural since we represent the diode just as an impedance  $Z$ . The switch has different states, ON and OFF states. Correspondingly, the impedance of diode would appear two different levels under different bias conditions. For example, when the switch is at ON state, the impedance of the diode would be low impedance under forward biasing for series configured reflective switch. For ideal cases, the  $Z$  approaches zero so that the ideal insertion loss (3.1) of series configured switch is 1 (in linear scale). On the other hand, when the series configured switch is at OFF state, the impedance of the diode would become high impedance under reverse biasing. Then, the isolation (the same equation 3.1) would be infinite (in linear scale) by setting  $Z$  infinity in ideal cases.

For shunt configured switch, when the switch is at ON state, the admittance of the diode should be zero in ideal cases. The similar analysis could be done by inspecting the insertion loss (3.2) by setting  $Y$  zero. For OFF state, the admittance of the diode should be infinite so that the ideal isolation would be infinite. The same validation could be done by setting  $Y$  infinite in (3.2).

The series-shunt switch is the combination of the series and the shunt configuration. The same analysis could be done by inspecting the equation (3.3). We can discover that the series or the shunt configured switch is one of the special cases by letting  $Z_{sh}$  infinite or  $Z_{se}$  zero.

The mechanism of switch is done by different level of impedance of diode. Thus, the measurement of the impedance of the diode under forward and reverse biasing would be the first step. The switch for vehicle-collision-avoidance-radar-system doesn't need to handle high power, so the diode used for the switch would be the

same GaAs Schottky diode as frequency doubler used. Besides, the fast switching speed of GaAs Schottky diode switch is suitable for radar systems. Fig3-4 indicates the measured impedance of the GaAs Schottky diode under forward and reverse biasing individually.

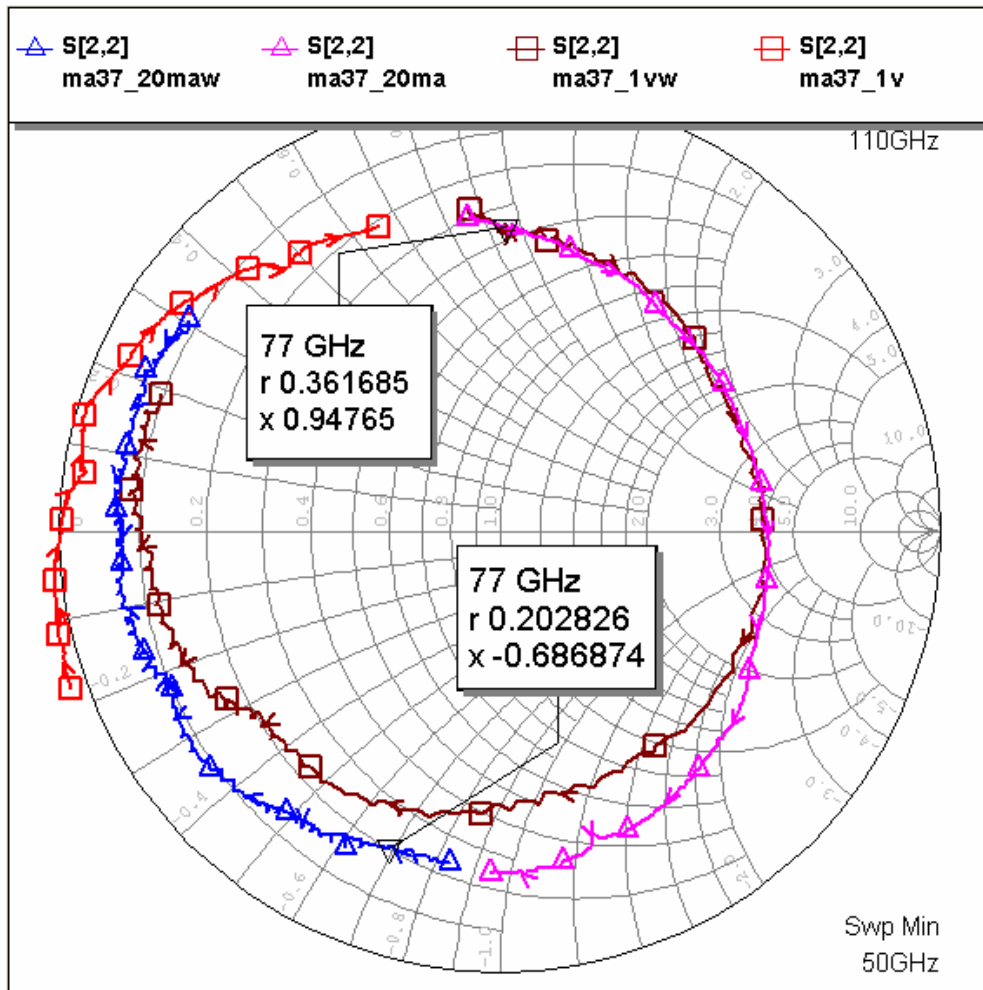


Fig3-4 Measured impedance of Schottky diode under forward and reverse biasing

Fig3-4 depicts the measured impedances under two different biasing from 50GHz to 110GHz. The forward biasing is defined when the current of diode is 20mA and the reverse biasing is defined as the reverse applying voltage is 1V. The measurement was done by a Agilent 8510 network analyzer with waveguide measuring head. Slightly jump between V-band and W-band measurement is observed due to unavoidable measurement error. The normalized impedances of forward and reverse biasing at 77GHz is about  $(0.2-0.69j) \Omega$  and  $(0.36+0.95j) \Omega$ . Take these values into (3.1) and (3.2). The insertion loss and isolation for series configuration could be derived as 1.24dB and 2.09dB correspondingly. For shunt configuration, the insertion loss and isolation are 2.027dB and 2.76dB respectively. It is apparent that the insertion loss for each configuration is still acceptable but the isolation is too terrible. The reason why the switch performs awfully at OFF state is that the impedance at reverse biasing is not high enough. Thus, the diode couldn't be used directly for series or shunt configuration. Matching network must be inserted to make the impedance as high (or low) as possible at OFF (or ON) state. The matching network can be realized in the following procedures.

First, apply matching network so that the impedances of forward and reverse biasing are, complex conjugate pairs, symmetrical to the real axis in the Smith chart as Fig3-5 shows. Second, add a quarter-wavelength transformer to the matching network to transform two impedances with  $180^\circ$  difference like Fig3-6. Finally, the matching is completed by rotating these two impedances to real axis with a one-eighth wavelength transmission line. Fig3-7 depicts the final impedances of forward and reverse biasing. The high and low impedances are around  $0.14\Omega$  and  $5.34\Omega$  at ON and OFF state. The insertion loss and isolation are correspondingly 0.588dB and 11.3dB based on (3.1).

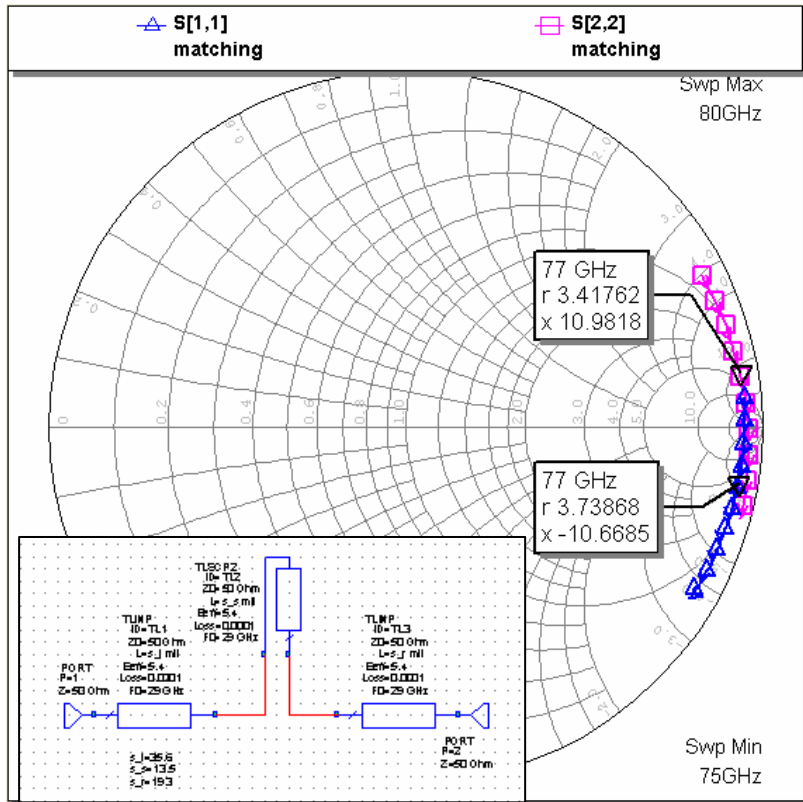


Fig3-5 Complex conjugate pairs in the Smith chart

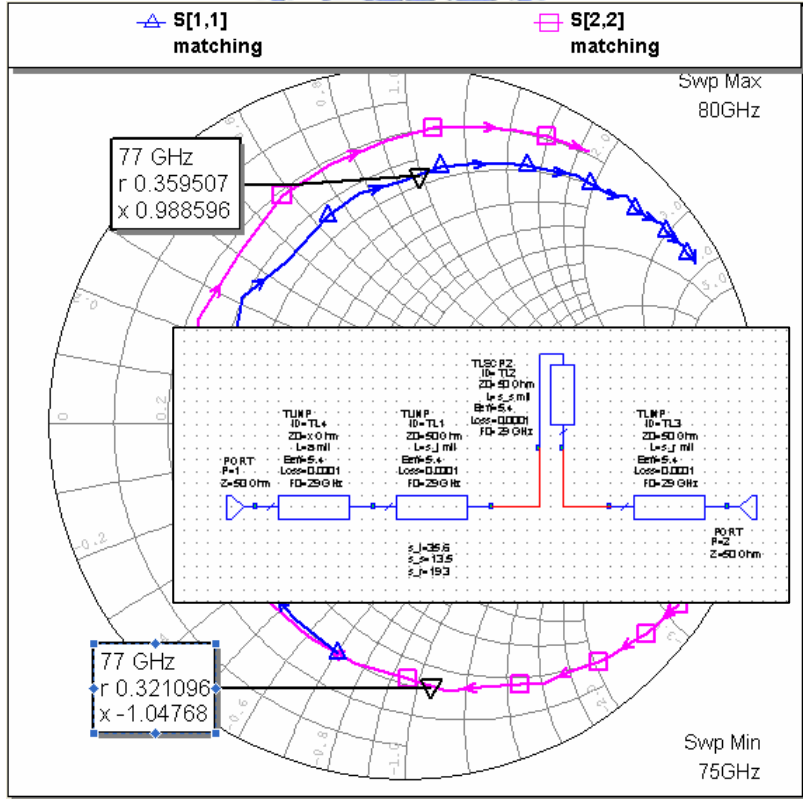


Fig3-6 Transformed impedances with 180° difference



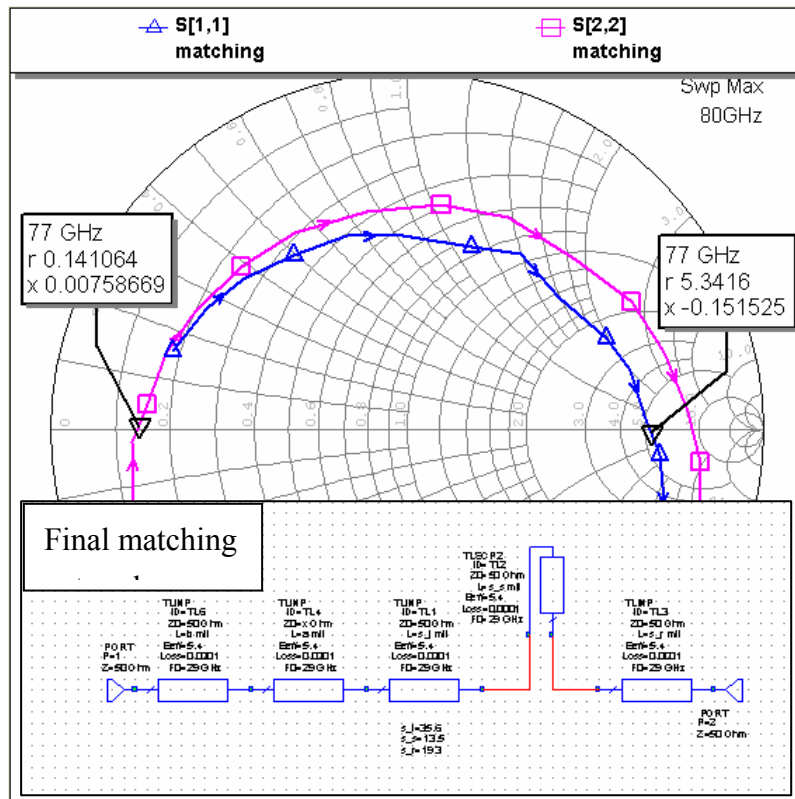


Fig3-7 Final impedance of forward and reverse biasing

The switch applied with matching network could have acceptable performance in both insertion loss and isolation. The next step would be the implementation of the needed matching network. The matching network is mainly composed of transmission line and shunt open stub. Both of them have the same impedance which is constructed from 3mil wide line width and 1.4mil wide gap spacing. The matching network is simulated in 3-D full-wave simulator HFSS, as Fig3-8 depicts.

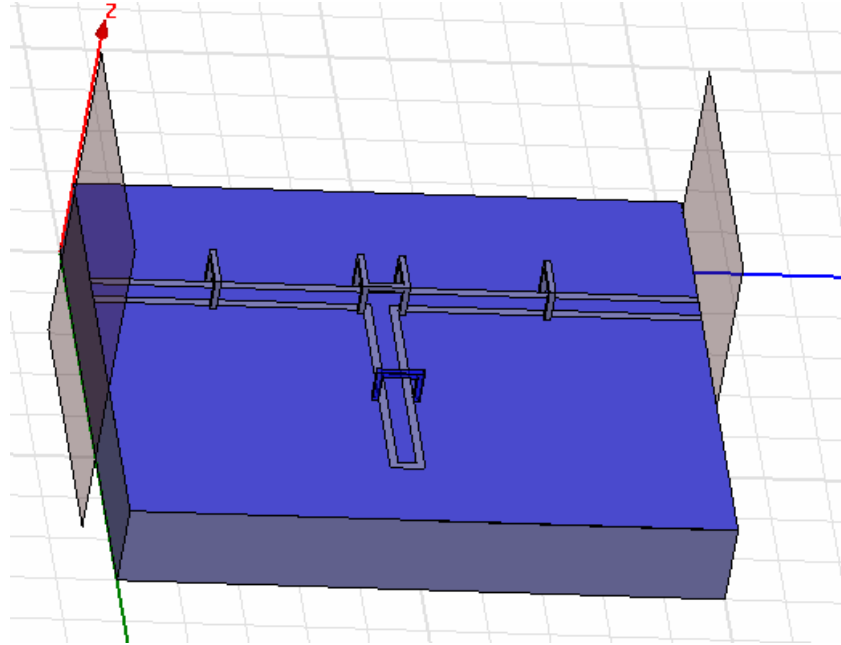


Fig3-8 Simulated matching network in HFSS

In fact, the open stub has a small capacitance due to the fringing field at the open end which is reported in [9]. Besides, the parasitic effects of T-junction and bond wire should also be considered. Therefore, fine adjustment must be done for circuit simulation. The fitting curve is shown in Fig3-10. Then, the shunt configured SPST and SPDT could be realized utilizing the simulated matching network as Fig3-11 and Fig3-12 show.

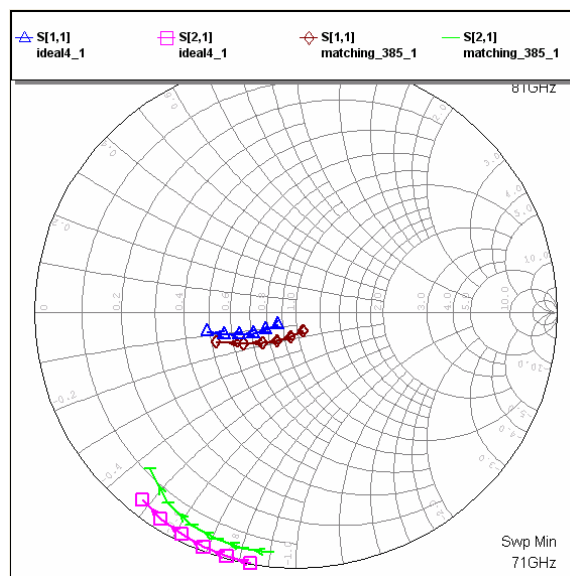
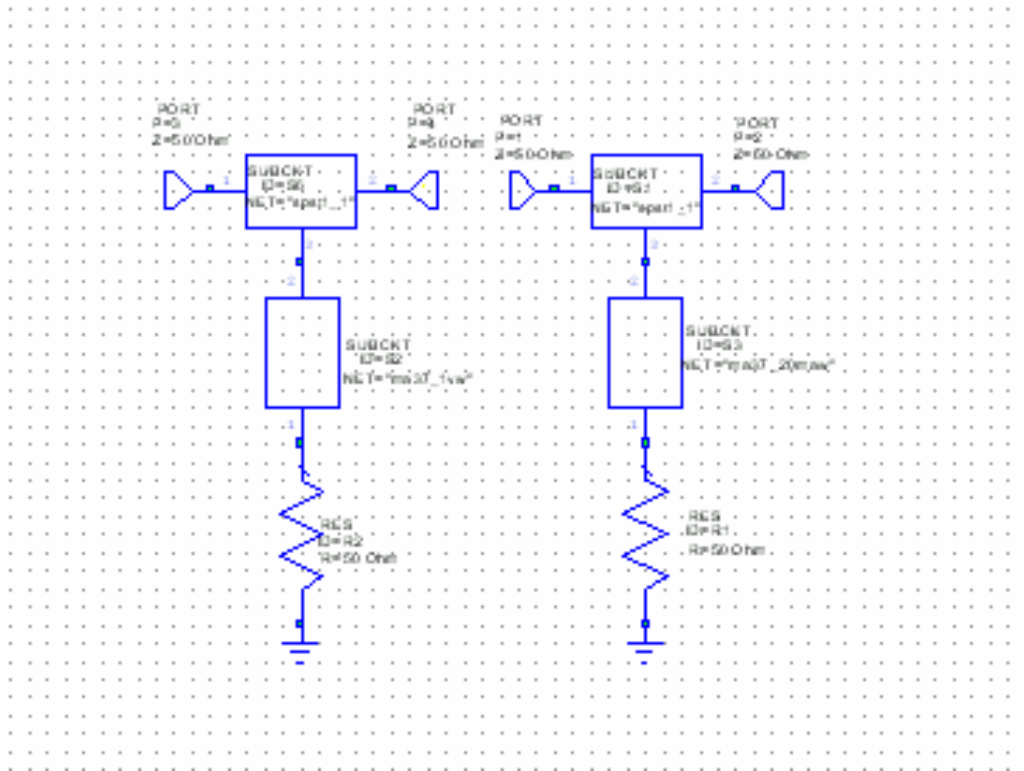
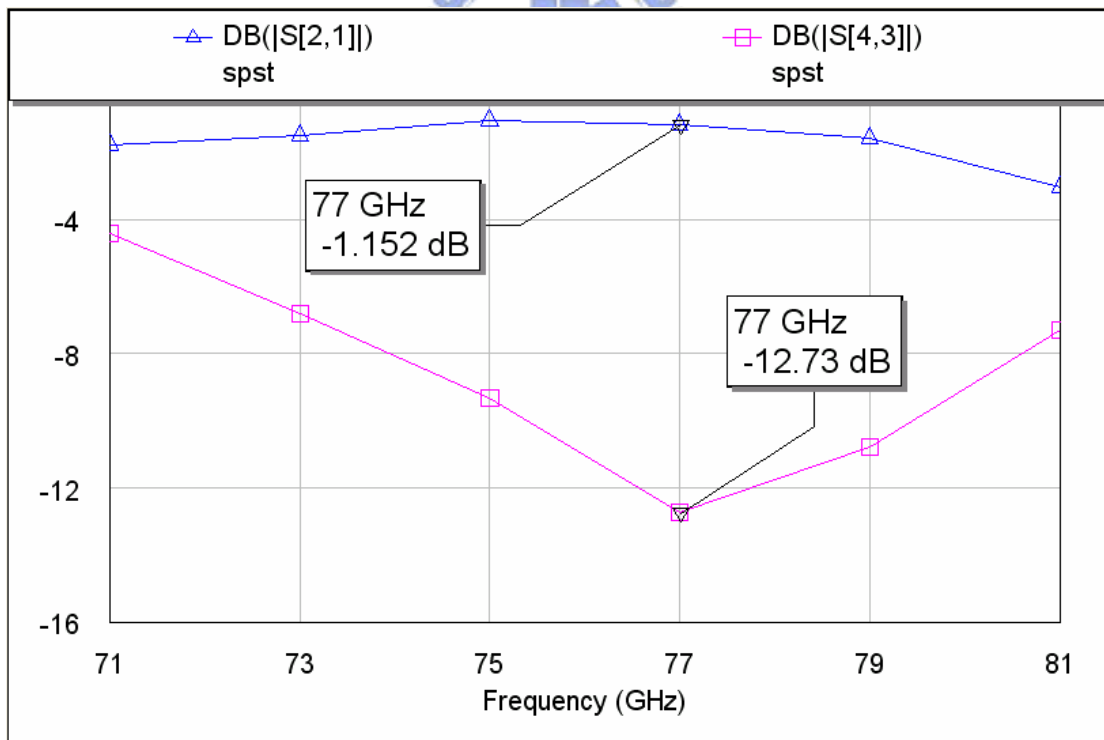


Fig3-9 Curve fitting between ideal and practical matching network

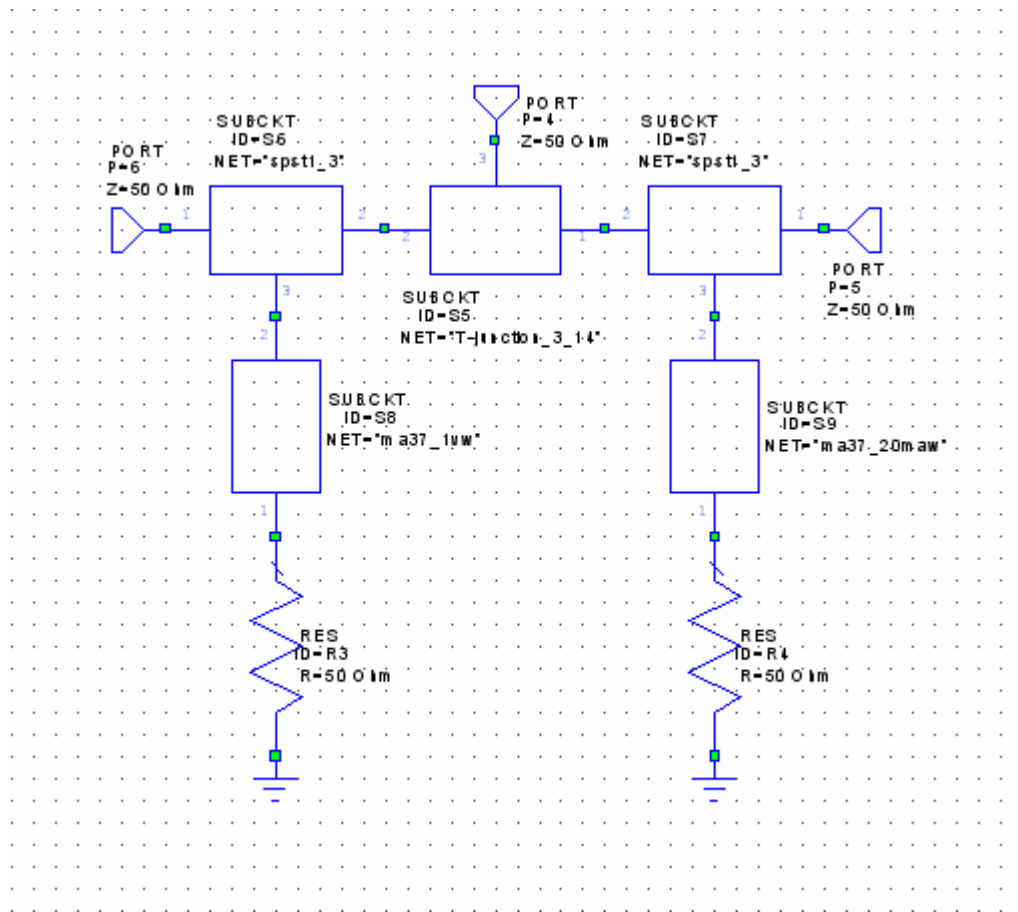


(a) SPST simulation

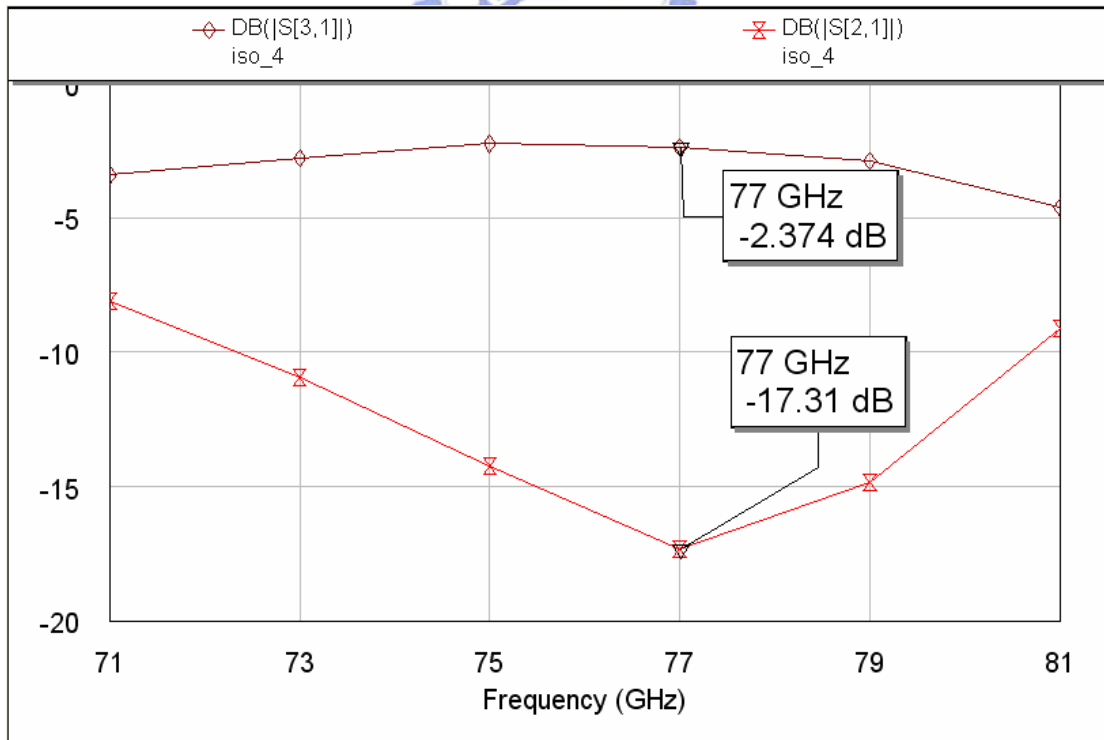


(a) Simulated insertion loss and isolation of SPST

Fig3-10 Shunt configured SPST simulation



(a) SPDT simulation

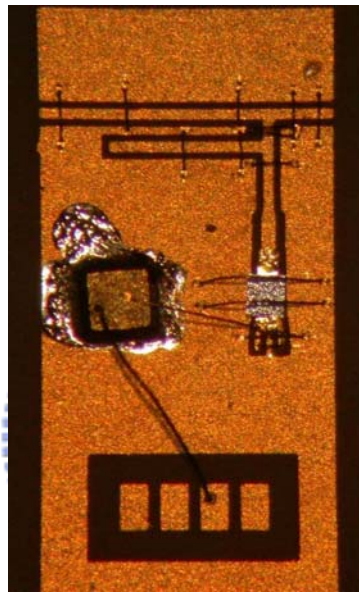


(a) Simulated insertion loss and isolation of SPDT

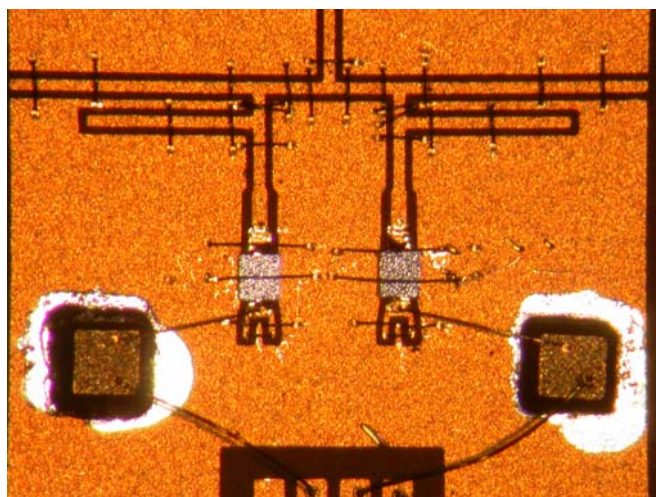
Fig3-11 Shunt configured SPDT simulation

### 3.2 Circuit implementation and measurement

Fig3-13 indicates the circuit layouts and measurements of SPST and SPDT. The circuit sizes of them are 73mil x150mil and 150mil x150mil separately. The DC bias is applied to diodes through a low-pass filter which is formed by two long bond wires and a metal-insulator-metal capacitor. Additionally, a long bond wire, which behaves high reactance at RF, is needed for DC ground.



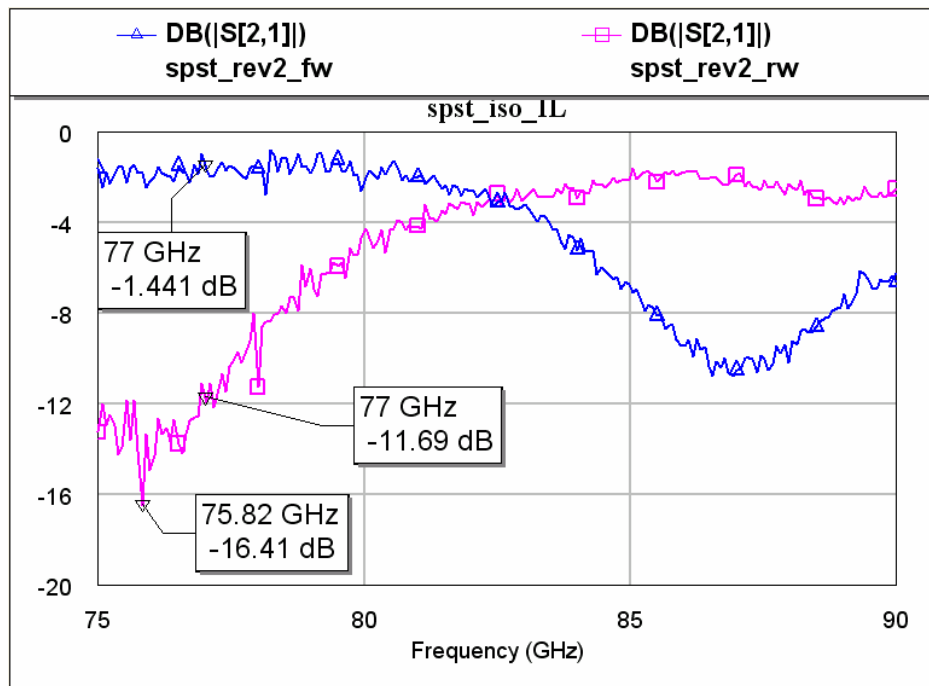
(a) Shunt configured SPST



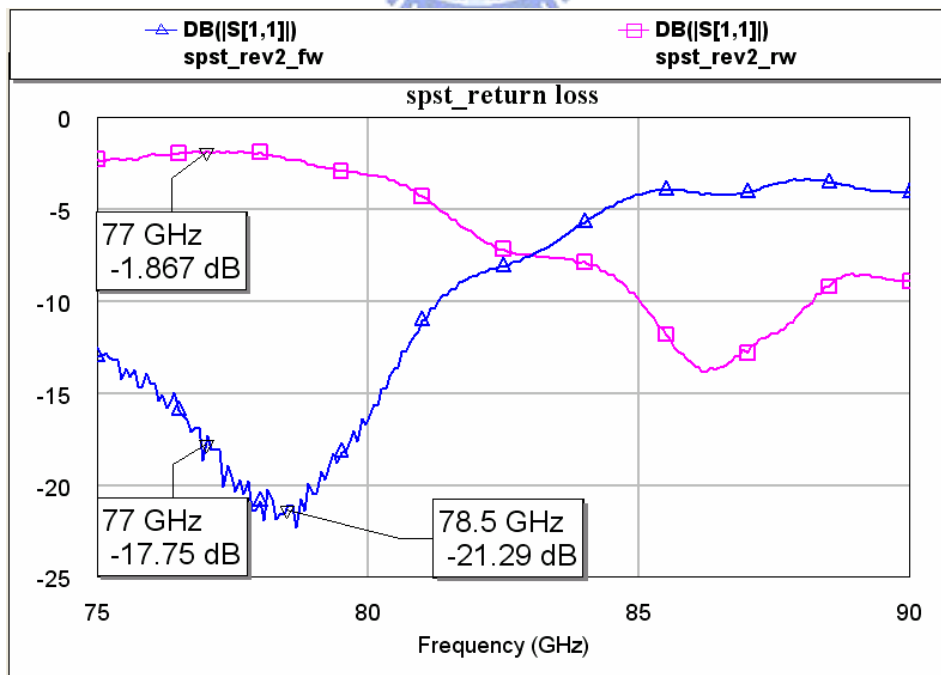
(b) Shunt configured SPDT

Fig3-12 Physical layout of shunt configured SPST and SPDT

The SPST and SPDT are measured by a probe station. Fig3-14 and Fig3-15 indicate the measured results of the ON and OFF states of them. A 50Ω termination is required when SPDT is measured.

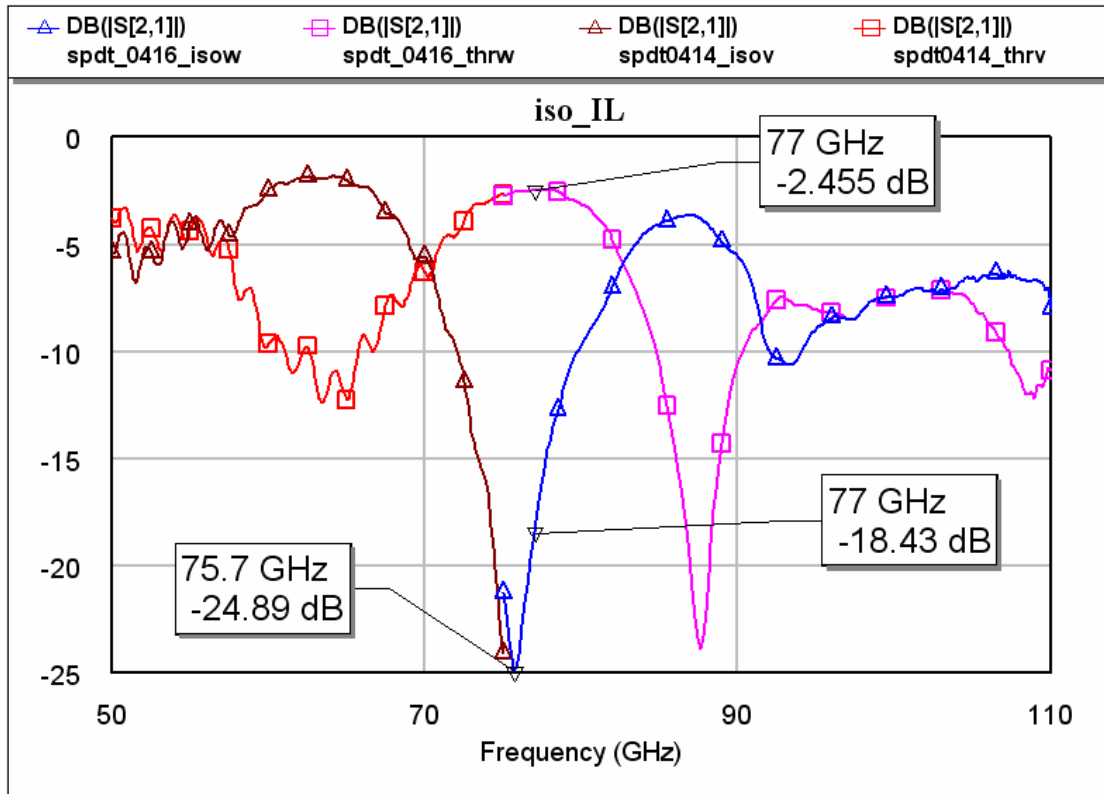


(a) Measured isolation and insertion loss of shunt configured SPST

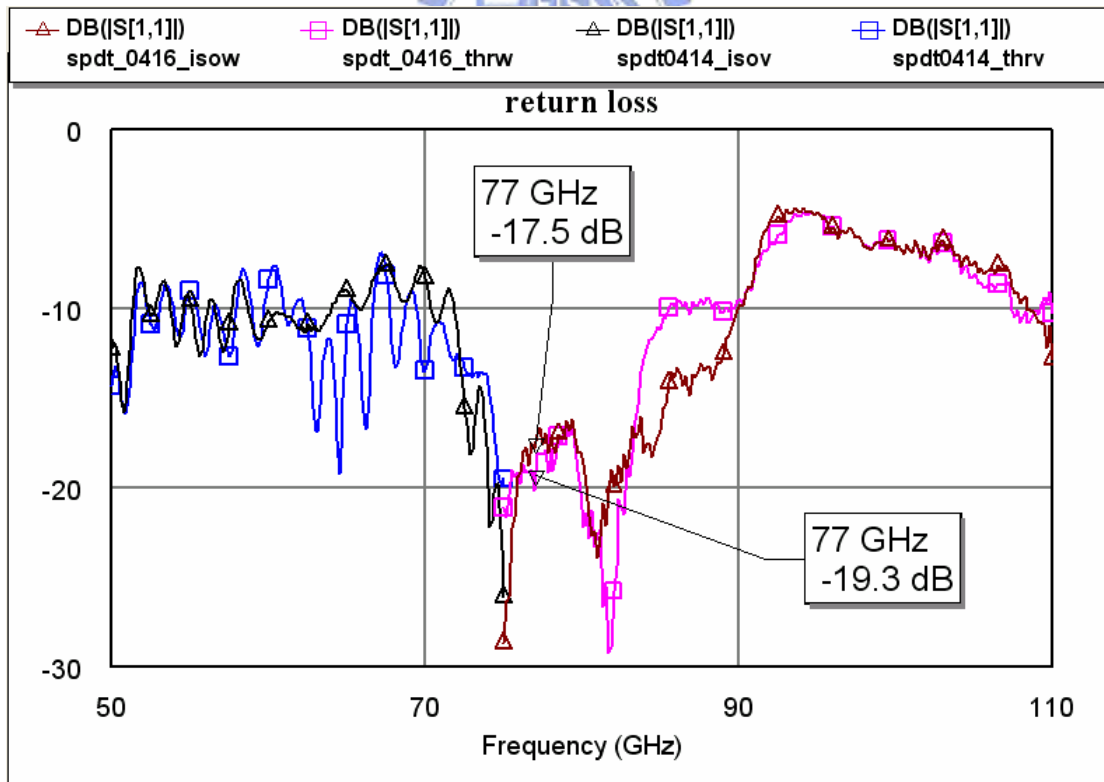


(b) Measured return loss at ON and OFF state of shunt configured SPST

Fig3-13 Measurement of shunt configured SPST



(a) Measured isolation and insertion loss of shunt configured SPDT



(b) Measured return loss at ON and OFF state of shunt configured SPDT

Fig3-14 Measurement of shunt configured SPDT

The measured insertion loss and isolation of SPST are 1.44dB and 11.69dB at 77GHz separately. The best isolation, 16.41dB, occurs at 75.8GHz. Although slightly frequency shift exists between simulation and measurement, the calculation value, circuit simulation, and measurement of shunt configured SPST do not differ from each other very much as Table I shows. The return losses of the ON and OFF state are 17.75dB and 1.867dB at 77GHz respectively. The worse return loss at OFF state is due to the reflective type switch configuration.

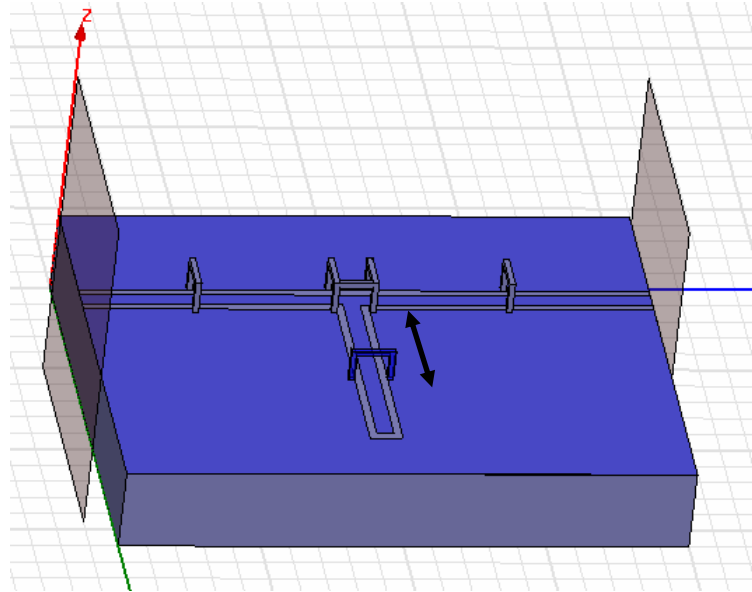
Table I Insertion loss and isolation comparison

	Insertion loss(dB)	Isolation(dB)
Calculation value	0.588	11.3
Circuit simulation	1.152	12.73
Measurement	1.44	16.41

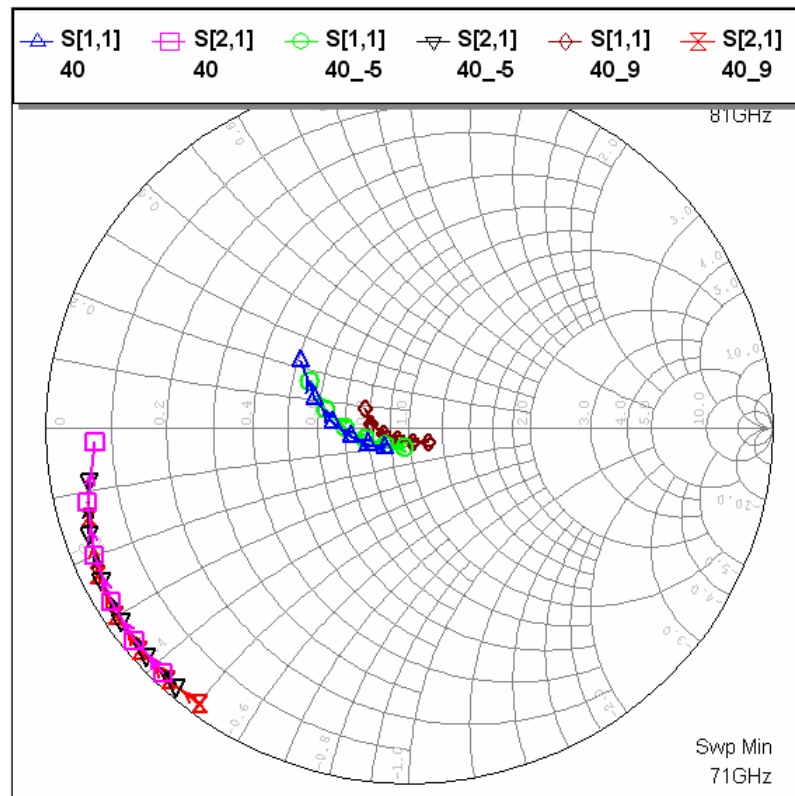
The measured insertion loss and isolation of SPDT are 2.455dB and 18.43dB at 77GHz individually. The best isolation, 24.89dB, occurs at 75.7GHz. The return loss should be the same for SPDT since there are always one ON path and one OFF path. The return loss is about 18dB at 77GHz.

While it seems that the simulation in HFSS is credible in implementation of switch, one important subject should be noted here for CPW simulation. The bond wire parasitic effect is not negligible about the size, location, height, and coupling effect of the bond wire. For instance, the different location of bond wire would result in different simulation results as Fig 3-16 shows. As a result, the implementation and simulation layout should closely coincide with each other.





(a) Location Variation of bond wire



(b) Various simulation result correspond to different bond wire location

Fig3-15 The effect of the bond wire location

## Chapter 4 Conclusion

In this thesis, two circuit components, frequency doubler and switch for vehicle-collision-avoidance-radar-system are presented. Table II and Table III summarize the performance of these circuits respectively.

Table II The performance of frequency doubler of different circuit structures

	Conversion loss at 77GHz	Bandwidth	Required LO power	Circuit size
Rat-race ring (reverse direction)	13.4dB	25GHz~87GHz	11dBm	95mil x 116mil
CPW-CPS balun (same direction)	13.96dB	<20GHz~82GHz	15dBm	70mil x 91mil
CPW balun (same direction)	16.8dB	<20GHz~55GHz	>15dBm	100mil x 66mil

From Table II, we can discover that the most suitable circuit structure for the frequency doubler is rat-race ring due to its good conversion loss and smaller required LO power. The collision-avoidance-system does not require broad bandwidth. Thus, bandwidth is not considered here.

Table III The performance of shunt configured SPST and SPDT

	Insertion loss	Isolation	Return loss
SPST	1.44dB	11.69dB	17.75dB
SPDT	2.455dB	18.43dB	18dB

The performance about switch indicated in Table III is acceptable but some improvement still has to be done to adjust the frequency shift.

- [1] Rainee N. Simon, *Coplanar Waveguide circuits, Componentes, and Systems*, John Wiley & Sons, N. Y. 2001.
- [2] David Pozar, *Microwave Engineering*, 2<sup>nd</sup> Edition, John Wiley & Sons, N. Y. 1998.
- [3] S. March, "A wide-band stripline hybrid ring," *IEEE Trans. Microwave Theory Tech.*, vol. MTT-16, p. 361, June 1968.
- [4] L. Fun, S. Kanamaluru, and K. Chang, "A new wide-band and reduced-size uniplanar magic-T's," in *IEEE MTT-S Int. Microwave Symp. Dig.*, 1995, pp.667-670
- [5] Chi-Yang Chang, and Chu-Chen Yang, "A novel broad-band chebyshev response rat-race ring coupler," *IEEE Trans. MTT.*, vol.47, April 1999.
- [6] Chi-Hao Lai, "Uniplanar W-band mixers and doublers," 單平面式 W-頻段混波器與倍頻器, 交通大學電信研究所 2002.
- [7] H. K. Chiou, C. Y. Chang, and H. H. Lin, "Balun design for uniplanar broad band double balanced mixer," *Electronics Letters*, Vol. 31, No.24, pp.2113-2114, Nov 1995.
- [8] M. J. Hsieh, C. Y. Wu, C. Y. Chang, and D. C. Niu, "Broadband mm-wave Schottky diode frequency doubler using a broadband CPW balun," *TSMMW2004*
- [9] Beilenhoff, K.; Klingbeil, H.; Heinrich, W.; Hartnagel, H.L.; Open and short circuits in coplanar MMIC's, *Microwave Theory and Techniques, IEEE Transactions on* , Volume: 41 , Issue: 9 , Sept. 1993, Pages:1534 – 1537

[10] Kai Chang, Inder Bahl, Vijay Nair, *RF and Microwave Circuit and Component Design for Wireless Systems*, Chapter 7

